# Coupling of Solvent-free synthesis and reactive extrusion of alumina: an ecologically efficient integration for heterogenous catalysts synthesis

*AUTHOR NAMES*

*Pierre-Igor Dassie [‡1], Ryma Haddad [‡1], Maud Lenez[1], Alexandra Chaumonnot[2], Malika Boualleg[2], Patrick Legriel[1], Ales Styskalik[4], Bernard Haye[1], Mohamed Selmane[3], Damien P. Debecker[4], Clement Sanchez[1], Corinne Chaneac[1] and Cedric Boissiere[1]*.*

AUTHOR ADDRESS

1. Laboratoire de Chimie de la Matière Condensée de Paris (LCMCP), Collège de France Sorbonne Université, CNRS, 4 Place Jussieu, 75252 Paris, France.
2. IFP Energies Nouvelles (IFPEN), BP 3, F-69360 Solaize, France.
3. Fédération de Chimie et Matériaux de Paris-Centre (FCMat) Sorbonne Université, Paris France.
4. Institute of Condensed Matter and Nanosciences (IMCN), Université catholique de Louvain (UCLouvain), Place Louis Pasteur, 1, 1348 Louvain-La-Neuve, Belgium).

KEYWORDS

Sol-gel, Solvent-free, Green synthesis, Reactive extrusion, Alumina, Boehmite Catalysts.

**ABSTRACT**

Innovating in materials manufacturing processes is a challenge to reduce the environmental impact of the chemical industry in line with sustainable development objectives, such as promote sustainable industrialization, and ensure responsible consumption and production patterns. One of the ways to reach this goal is to revisit the main synthesis processes and to rethink their use. Reactive extrusion is a well-known continuous process used to produce and shape various materials in the field of polymer and food industries, but hardly any for the direct synthesis and shaping of metal oxide materials (ceramics). By contrast, sol-gel chemistry offers tremendous opportunities to synthesize metal oxide networks by polycondensation of molecular precursors at low temperature, but it is mostly operated in sluggish batch processes, using massive amounts of solvent contaminants, and producing large amounts of chemical wastes (E-factor > 40). In this work, for the first time, we coupled extrusion with sol-gel chemistry to produce high surface area shaped alumina-based materials that meet or exceed the requirements to be used as heterogeneous catalysts or catalyst supports. The necessity to adapt sol-gel chemistry – usually done in diluted environment – to meet the twin-extruder technical constraints – usually working in viscous environment – led to a peculiar choice of reaction conditions little discussed in the literature: the hydrolysis/condensation of (solid) alkoxide precursors without solvent. We were able to synthetize and shape high specific surface area boehmite (γ-AlOOH), at room temperature, in a continuous mode, and in solvent-free conditions. The solids are directly shaped in the form of self-standing "spaghetti" or extrudates. Upon calcination, the shaped hydroxides are converted into mesoporous and high specific surface area gamma alumina ($\gamma$-$Al_2O_3$) materials. We show that such materials display high catalytic activity in the dehydration of ethanol. The process intensification presented here paves the way to very low-waste, low-energy, and – all in all – more sustainable

manufacturing practices toward shaped high surface area metal oxides. In addition, it could be potentially less expensive since the simplification of the equipment and the lower energy consumption will contribute to drastically reduce the production costs even if the reagents are more expensive.

## INTRODUCTION

Catalysts are an essential cornerstone of industrial chemistry, especially for sustainable chemical processes development since they allow massive production of chemical commodity for a lower cost. They are used in many fields: energy [1,2], environment [3–5] and materials [2,6].

Heterogeneous catalysts are favored whenever possible for they allow performing the same reaction multiple times, with lower energy input and, in some cases, they can be operated in continuous flow mode, for long time on stream [7–9]. Their structure and composition can be complex according to the targeted reaction. They are usually made of an active phase dispersed onto a mechanically and chemically robust porous support. The shape of the support is adapted to the type of the reactor, it can be powders, extrudates, monoliths, etc [9–13].

While efficient heterogeneous catalysts are essential to develop effective and sustainable chemical processes, the environmental and economic burden of their preparation itself must also be considered in the evaluation of any proposed catalytic technology [14]. The preparation of catalysts and catalyst supports usually requires multi-steps synthesis to control textural and mechanical properties that generate large amounts of (liquid and gaseous) wastes and are often energy intensive. Gamma alumina ($\gamma$-$Al_2O_3$) is one of the more representative support catalysts from the family of transition alumina that can be produced efficiently and reproducibly, with controlled size and shape, by topotactic dehydration of $\gamma$-AlOOH (boehmite). $\gamma$-$Al_2O_3$ is

commonly used as catalyst support at the industrial scale for oil refinery, especially for reforming [15,16], hydro-treatment [17] and hydro-conversion [18] reactions and also for alcohol dehydration to alkenes and in the Claus process [19,20]. γ-$Al_2O_3$'s interest resides in its highly modular textural properties, which can be tuned by the size and morphology of primary boehmite particles, their shaping process (peptization and neutralization steps), as well as its quite low reactivity coupled with a good mechanical strength [21–23].

The preparation of ready-to-use alumina-based catalysts is a long and quite expensive process including at first several steps for the boehmite nanoparticle synthesis and in a second time a shaping process as illustrated figure 1 [24,25]. Boehmite conventional synthesis protocols imply a multi-step approach depending on the synthesis strategy. The sol-gel method, also known as the Yoldas process, uses metal alkoxides as precursors with an excess of water ($H_2O$/Al is around 200/1)[26]. In industry, the most common strategy is the neutralization of an aqueous acidic solution of metal salt precursors (such as $Al(NO_3)_3$ [27–29], $Al_2SO_4$ [29–31], or $AlCl_3$ [32]) by a basic solution of aluminate [33], NaOH [28], ammonia [29] or urea [29,31]. As obtained precipitate corresponding to boehmite is usually aged in the mother liquor at atmospheric or higher pressure, at different temperature (from room temperature to 150 °C) [28,34]. Afterward, the solid is filtered from the reaction medium, and washed several times with a large amount of water, at room temperature or higher, to eliminate the counter-ions from the aluminum salts. Then the wet powder, named "filtration cake", is dried in an oven. Apart from precisely controlling the texture, crystalline structure, and surface properties of the alumina powders, catalysis scientists must also consider the shaping of the latter into larger catalysts bodies (microsphere, extrudates, monolith, etc.) that can be handled easily and loaded in flow reactors without causing excessive pressure-drop [35–38]. This kneading-extrusion process includes the peptization of the powder in a liquid, usually acid or base

and potentially with organic or mineral additive before extrusion. Peptization leads to a de-agglomeration of particles due to electrostatic repulsions of charged surface after adsorption of protons or hydroxyl ions. Finally, in order to transform the boehmite into γ-$Al_2O_3$ a calcination step is applied, usually between 500 to 700 °C [39,40]. The final textural properties of the support are mainly set during boehmite synthesis, but it can be modulated to a certain degree during the shaping process [35].

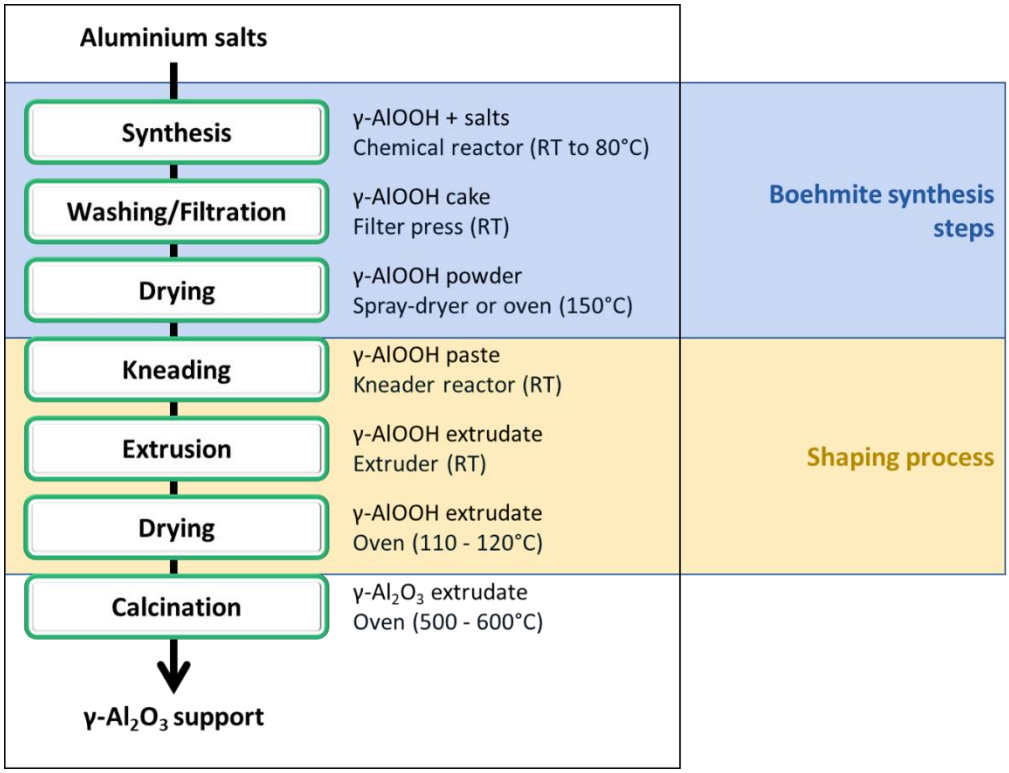


**Fig. 1**. Schematic view of a conventional, multi-step [21,34], production route for γ-$Al_2O_3$ catalyst support from aluminum salts according to Industry. RT stands for Room Temperature

As depicted in figure 1, before calcination, at least six elementary steps are necessary to get γ-$Al_2O_3$ shaped extrudates via the conventional precipitation methods. Each step requires a different device, different temperature and different completion times. In most cases, each step is carried out in a batch mode. One of the many consequences of this processing pathway is that a very large

volume of solvent (mostly water) is spent. Also, binding agent [41] and porogen can be added in order to improve respectively extrudates cohesion before thermal treatment and to reach required textural properties. Based on rare published reports [42,43] the production of γ-$Al_2O_3$ extrudates produces a lot of liquid wastes. In the literature the weight of effluents generated by the washing of aluminum counter ions is rarely quantified (from our experience, several times the same amount of, sometimes hot, water used for precipitation). Furthermore, the overall production process is discontinuous. This conventional approach, is highly unsatisfactory from a sustainability point of view: poor atom economy, large waste production (high E-factor), and high energy consumption.

A possible way to tackle this problem is to regroup as many steps as possible into one single device, using a drastic economy of atoms and energy. With this later considerations, reactive extrusion is an interesting process to develop for the intensive production of such catalysts. First, the extrusion process is a shaping process, well-known in the industry and widely used to shape metal oxide catalysts or catalyst supports such as γ-$Al_2O_3$. Reactive extrusion process is about using a continuous extruder as chemical reactor as well as a shaping tool. Indeed, it is a chemical reactor with a large contact surface area able to transfer heat to/from the reactive medium. The modularity of its screw profile allows performing transport, mixing, and shearing of matter; and it can accommodate highly viscous media. Reactive extrusion has been used for a long time for organic polymerization or polymer modifications [44,45] in industrial field [45]. Its recent development is focused on hybrid materials [44,46]. Despite its obvious potential for synthesis and shaping of metal oxides materials, like γ-AlOOH boehmite, no information has been published on the subject to our knowledge.

In this paper, the production of shaped gamma alumina is revisited by combining extrusion process with Sol-Gel chemistry [47], which is known for its ability to produce metal oxides in mild

experimental conditions and its adaptability to industrial processing. Intrinsically, aluminum-based sol-gel reactions require large amounts of heated solvent to control hydrolysis and condensations steps, and lead to boehmite particles of controlled shape and size which are crucial for obtaining highly porous active and selective catalysts [26,48–51]. In the literature, the precipitation of boehmite from aluminum alkoxide precursors uses also large amounts of solvent for controlling the high reactivity and exothermicity of the hydrolysis step [26]. By contrast, a few recent scholarly publications[40,52–58] mention the facile synthesis of boehmite at ambient temperature by using a solvent free synthesis in which a very small amount of water, used as a reactant, is ground into a hand mortar with aluminum alkoxides. These reports focused on the final characteristics of the γ-$Al_2O_3$ particles obtained after calcination but no investigation was presented on the properties of the boehmite intermediates or on the influence of processing parameters. More specifically, the high exothermicity of alkoxide hydrolysis reaction was not discussed, even though it is likely to strongly influence the final product characteristics for the reaction temperature depends on the amount of matter reacted at a time. Looking for strategy allowing eliminating liquid waste completely, we concluded that the direct use of alkoxide precursors in a solvent-free reaction can be an efficient synthesis approach.

Here, we disclose for the first time a solvent-free, binder free, and porogen-free synthesis and shaping strategy of high surface area mesoporous γ-AlOOH extrudates with a near ambient temperature, one-step-one-tool process of reactive extrusion. After calcination, γ-AlOOH extrudates lead to γ-$Al_2O_3$ with high specific surface area and porous volume. As a reference, extrudates are also prepared from boehmite particles obtained in the same chemical conditions but using a batch process following by a usual kneading-extrusion processes (including

peptization/neutralization steps). The obtained γ-$Al_2O_3$ extrudates were tested for alcohol dehydration reaction and compared to a commercial alumina powder.

## MATERIALS AND METHODS

### Chemicals

Chemical as follows were used; Aluminum tri-Sec-Butoxide (ASB) 97% from Sigma-Aldrich, Aluminum IsoPropoxide (AIP) 98% from Sigma-Aldrich. Milli-Q water was used for alkoxide hydrolysis. AIP was grinded with a mortar before used (the grinded powder is analyzed before use by FTIR spectroscopy to ensure that it wasn't hydrolyzed/condensed during grinding or storage). A commercial boehmite (PuralSB3) coming from Sigma-Aldrich is also used as reference for characterization.

### Reactive extrusion of γ-AlOOH mesoporous extrudates

Scamex's Twin Screws Micro-Extruder (TSME) of 60 cm length, with 18 mm diameter screws was used. Temperature device was set at 30 °C (corresponds to room temperature during summer time) and the screws speed at 300 rpm. The screws profile of the mixing area (figure SI.1 B) was selected by comparing kneading, transport, and mixing modulus in term of textural properties of the materials produced at various temperatures and hydrolysis rates (experiments not presented here). We selected the kneading profile that gave boehmite with highly reproducible surface area and porous volume and that was reasonably stable with hydrolysis rate variations and aluminum alkoxide source.". Water was fed through the hopper, (H2 in figure SI.1 A), using a peristaltic pump at 1.32 and 1.76 ml/min (corresponding respectively to a water/ aluminum molar hydrolysis

ratio “h” of 6 and 8). AIP was fed by doser through the next hopper (H3 in figure SI.1 A), which is closest to the head extruder, with a constant feed of 2.5 g/min. The feeding rate of aluminum alkoxide and water were chosen for producing as much boehmite as possible, while maintaining a constant water/alkoxide molar ratio. We determined the limit by increasing the doser feeding rate until the feeding hopper was blocked. Feeding rates provided in the manuscript are about 20% below the limit of our device. Mixing/shearing of AIP and water takes place between the third hopper and the die. It corresponds to a length of 18 cm along the screws, that includes three functional segments, one for transport, one for kneading and one for transport/compression, (figure SI.1 B). Samples are collected fifteen minutes after a solid come out from the extruder corresponding to the stabilization time. We checked that the production rate is constant without changing the appearance of the as-obtained material.

Reaction medium Minimum Residence Time (MRT) is measured by adding a dye, rhodamine B, with AIP through the third hopper H3. MRT is the time between the dye addition and a coloration appearance of the reaction medium extruded. For our samples MRT remained stable at 46-48 seconds.

**Mechanically-mixed Solvent-free synthesis of γ-AlO(OH) mesoporous powders (batch)**

Powder samples were prepared by mechanical mixing with an anchor, in a polypropylene bottle, for 10 minutes at 900 rpm at room temperature, 0.5 mol precursors (123.2 g of ASB or 102.1 g of AIP) with respectively 3 mol of water for ASB (h = 6) and 2.5 mol of water for AIP (h = 5). The cake was dried under vacuum for 14 hours at room temperature. Around 30 g of powder was produced for each precursor.

**γ-AlOOH mesoporous powder shaping into extrudates by kneading and extrusion**

Powder of each precursor obtain from a mechanically mixed Solvent-free synthesis was kneaded and underwent a peptization (addition of an acid solution, $HNO_3$) / neutralization (addition of a basic solution, $NH_4OH$) process to minimize aggregation defects and reach an adequate viscosity to allow shaping by extrusion. The kneading of boehmite powder was performed with a standard Kneader, aside from extrusion device. In a typical experiment 31 g of dry boehmite powder was introduced into a kneader. Then,20 mL of a nitric acid solution was added, to reach a $HNO_3$/Al molar ratio of 5%. After 105 min of kneading, 0.8 mL of $NH_4OH$ solution (3.73 M) and 3.3 mL of water were added, in order achieve a $NH_4OH/HNO_3$ molar ratio of 20%. Extrusion was performed with a press extruder and a trilob shape with a pressure in the 100-150 Bar range.

Extrudates samples prepared this way are labeled as follows: *Processing_Precursor_hydrolysis ratio_ post processing.* Processing can be either Kneading-extrusion (KE) or reactive extrusion (RE). For post-processing, fresh materials, dried materials and calcined materials are labeled (F), (D) and (C) respectively. For example, fresh extrudates prepared from IPA, with a hydrolysis ratio of 6 by reactive extrusion is labeled "RE_IPA_6_F", while a calcined extrudates made from an already prepared boehmite obtained with ASB using hydrolysis ratio of 5, and shaped in a second time by kneading followed by extrusion is labeled "KE_ASB_5_C".

**Characterization techniques**

*Fourier-Transform InfraRed* (FTIR) spectroscopy was carried out on a Spectrum 400 FT-IR/FT-NIR Spectrometer de PerkinElmer©. Attenuated Total Reflectance (ATR) measurement were done as follow: samples were scanned 16 times from 550 to 4000 $cm^{-1}$ with a resolution of 1 $cm^{-1}$, at room temperature. Transmittance measurements were done with KBr binder. Analysis procedure was 16 scans from 400 to 4000 $cm^{-1}$ with a resolution of 1 $cm^{-1}$, at room temperature.

*X-Ray Diffraction* (XRD) was carried out by a low angle diffractometer Bragg–Brentano Bruker D8 ADVANCE using filtered Cu Kα radiation over a 2θ range from 4° to 80° with a step size of 0.02°. To calculate an apparent size of the particles in all the hkl dimensions, the Scherrer equation was used.

*Scanning Electron Microscope* (SEM) was carried out by a Hitachi S-3400N.

*Transmission Electron Microscopy* (TEM) was carried out by a TECNAI 120 Spirit Twin at an acceleration voltage of 120.0 kV, with a Gatan Orius 1000 camera model.

*Nitrogen Physisorption* measurements were carried out by a BELSORP-max de MicrotracBEL©. Before the measurement, samples were degassed under a primary vacuum, (110 °C for 6 hours for boehmite and 250 °C for 3 hours for gamma alumina) to remove any adsorbed organic compounds and water. The Brunauer, Emmet, and Teller (BET) method was applied to determine the specific surface area and the BJH model was used for the determination of pore size distributions.

*The measurement of the crushing strength* was carried out with a servo-hydraulic testing system Instron 8502 (High Wycombe, UK), associated with a 5000 N load cell.

*Ethanol dehydration*

The catalytic tests were done as described by A. Styskalik *et al.* 2020.[59] The tests were carried out at atmospheric pressure, WHSV = 1.1 $h^{-1}$. The analysis temperature was varied stepwise (210, 255 and 315 °C). One step consisted of (i) heating ramp (5 °C $min^{-1}$) and stabilization at the set temperature (21 min) and (ii) steady temperature state (63 min). The catalysts were diluted with glass beads (0.5−1 mm) in order to keep the volume of the catalyst bed constant and silica beads

was added to fill the void of the reactor. The catalytic tests were performed with absolute ethanol, injected at a 0.212 g $h^{-1}$ rate using a NE-300 syringe pump in a 40 $cm^3$ $min^{-1}$ flow of $N_2$ (4.4 mol% of ethanol in $N_2$). The effluent gas was analyzed by a VARIAN 3800 Gas Chromatograph (9 injections at each temperature) equipped with a flame ionization detector (FID) and a Cydex B column (25 m long, internal diameter 0.22 mm, film thickness 0.25 μm).

## RESULTS AND DISCUSSION

So far, the one-step manufacturing of mesoporous γ-AlOOH extrudates remains essentially unexplored and was never reported. Industrially and in literature, synthesis and shaping of γ-AlOOH particles are carried out in separate steps. The final extrusion processing often requires a peptization/neutralization step performed by kneading to increase adhesive forces between compressed granules that form an extrudate. It removes the macroporosity coming from boehmite aggregates and insures the final product mechanical strength before calcination [41]. In one-step manufacturing of mesoporous γ-AlOOH extrudates without peptization, extrudates would hold together only by Van der Waals forces and hydrogen bonds, reducing considerably their ability to maintain shape and their mechanical strength after extrusion. Still, to go further with atom economy, we searched for a strategy to avoid the use of any binder. To safeguard mechanical integrity and cohesion between elementary boehmite crystals, we inferred that it would be more coherent to form them as much as possible after extrusion (in that way, the shear stress inside the device is not likely to break inter-crystal chemical bonds). Thus, the reactive medium (alumina precursor plus water) was extruded and pre-formed before the sol-gel condensation reaction was completed. In addition, this allows to control the residence time of the material in the device.

Following this train of thoughts, in order to reduce the observed reaction kinetics, chemical and processing parameters were adjusted in a way that allowed controlling the diffusion rates and minimizing the reaction medium residence time in the extruder: AIP was chosen as the sol-gel precursor. Theoretically, AIP, which is solid, is more reactive than ASB, which is liquid, but in a solvent-free reaction, AIP hydrolysis/condensation take more time than ASB due to its solid state (water diffusion into aluminum precursor's grains is much slower).

In this manuscript, we report reactive extrusions performed with two hydrolysis ratios (h = 6 and h = 8). Extrusion was not managed below a hydrolysis ratio of 6 due to extruder stuffing, and was not done above a hydrolysis ratio of 8 to avoid bayerite phase ($\alpha$-$Al(OH)_3$) formation as a co-product of boehmite, as it was observed by Huang *et al* [54]. Fresh extrudates obtained for a hydrolysis ratio of 6 and 8 are respectively named RE_AIP_6_F and RE_AIP_8_F.

To verify that reaction medium extrusion is done before the complete hydrolysis of AIP, freshly extruded product was analyzed by FTIR spectroscopy. The infrared spectra of AIP sol-gel precursor, freshly extruded RE_AIP_6_F and RE_AIP_8_F are shown in figure 2.

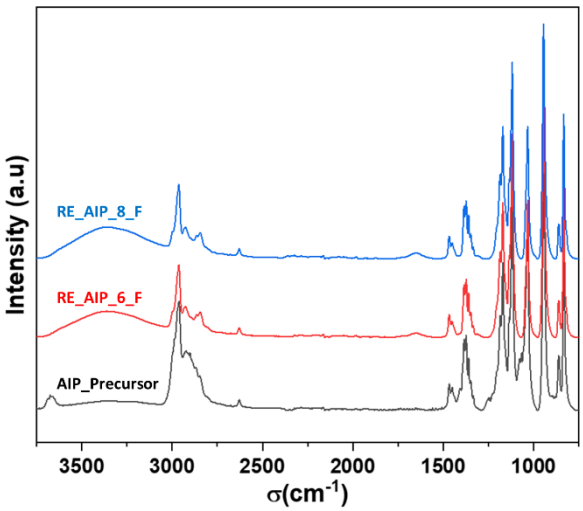


**Fig. 2**. Infrared spectra of AIP sol-gel precursor in black, RE_AIP_6_ F (freshly extruded with h=6) in red and RE_AIP_8_F (freshly extruded with h=8) in blue

Similar bands are observed in all three compounds. Most bands are associated to the isopropyl group: C-H stretching mode of the $CH_3$ and CH groups is between 2975 and 2850 $cm^{-1}$ [60], C-H bending and rocking modes between 1465 and 1340 $cm^{-1}$ and C-$CH_3$ stretching mode [61] with single band around 950 $cm^{-1}$. The C-O stretching mode is observed between 1100 and 1170 $cm^{-1}$. Bands at 860, 700, 674, 610 and 570 $cm^{-1}$ [62,63], are assigned to tetrahedral and octahedral Al-O vibration [64]. (Al)-O-C peak, characteristic of μ2-bonds of alkoxide is visible at 1033 $cm^{-1}$ [65], and is found in both extruded compounds, attesting that AIP hydrolysis is still in progress after extrusion. Finally, two peaks absent for AIP precursor, appear for RE_AIP_6_ F and RE_AIP_8_F: a large and intense band around 3330 $cm^{-1}$ assigned to water and alcohol O-H stretching mode, and a small band at 1645 $cm^{-1}$ assigned to water bending mode. Their appearance is expected since water is added to AIP as a reagent, and AIP hydrolysis generates isopropanol.

**Study of hydrolysis kinetic**

RE_AIP_8_F sample was analyzed by ATR FTIR spectroscopy after aging at room temperature for different time intervals (60, 90, 105 and 120 minutes). Infrared spectra are shown in figure 3. By comparing sample at 0 and 60 minutes after extrusion, the C-H stretching modes at 2975 and 2850 $cm^{-1}$ decrease fast if compared with the large band related to water, Al-OH and alcohol O-H stretching around 3000-3500 $cm^{-1}$ (the later decreases slowly with the progressive evaporation of alcohol). Bands of O-H bending mode at 1300 $cm^{-1}$ and C-O symmetric stretch at 815 $cm^{-1}$ corresponding to a characteristic band of isopropanol become visible. Most bands attributed to alkoxides have disappeared after 90 minutes including the μ2-Al-OC vibration at 1033 $cm^{-1}$, after 105 minutes. Complete hydrolysis of AIP is considered done at that time. No more change is observed afterwards.

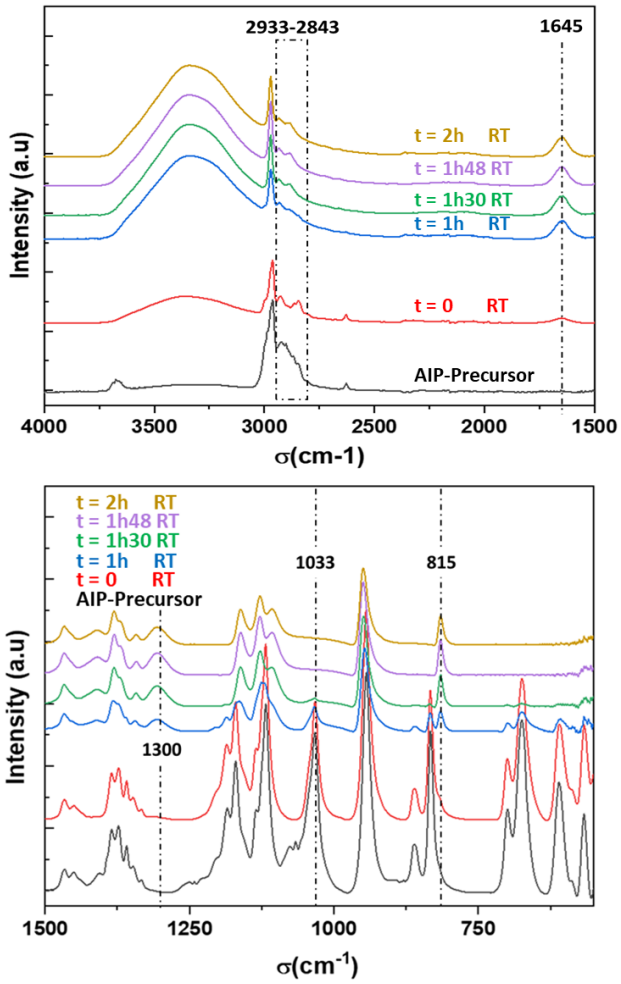


**Fig. 3.** Infrared spectra of RE_AIP_8_F sample as a function of time after reactive extrusion processing

## Study of condensation kinetic

RE_AIP_8_F sample was analyzed by XRD after aging in air at room temperature and at different time intervals, from one hour to 28 hours (figure 4). No diffraction peaks from AIP is visible (reference AIP XRD patterns provided in SI.2) [66], confirming that most of AIP is either hydrolyzed (this is coherent with FTIR data on hydrolysis kinetic) or not crystalline. The presence of very broad bands at diffraction angles close to those of boehmite material means that extrudates are made of low-ordered boehmite. From one to three hours of aging, slow boehmite structuration of

boehmite sheets is observed with the slow sharpening of boehmite diffraction peaks. From five hours of aging, the (020) diffraction peak characteristic of the stacking of boehmite sheets appears, meaning that the inorganic network starts its polymerization. This process goes on until no further evolution can be observed (after 28 hours of aging).

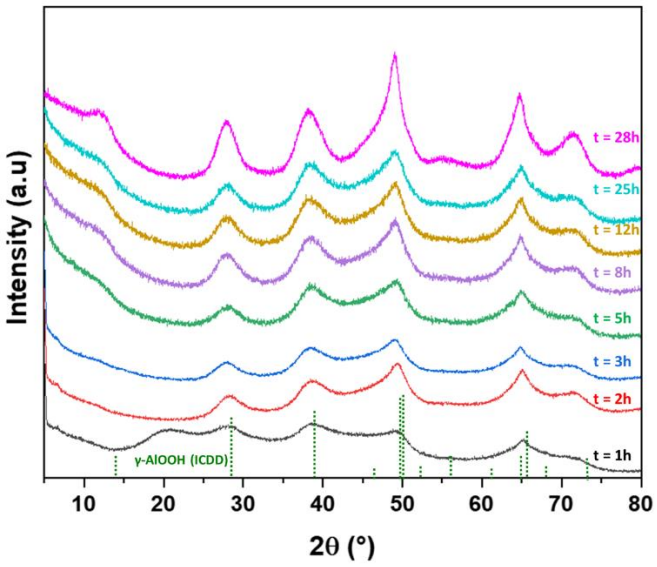


**Fig. 4.** XRD patterns of RE_AlP_8_F samples as function of resting time at room temperature after extrusion

**Structural analysis of extrudates**

For performing a reproducible structural study, four hours after synthesis we dried the samples under vacuum for removing remaining water and alcohol molecules and compared XRD patterns of RE_AIP_6_D and RE_AIP_8_D shown (figure 5). Both products show 6 broad peaks that can be indexed to the (020), (021), (130), (150), (132) and (152) characteristic plans of a nanometric boehmite phase.

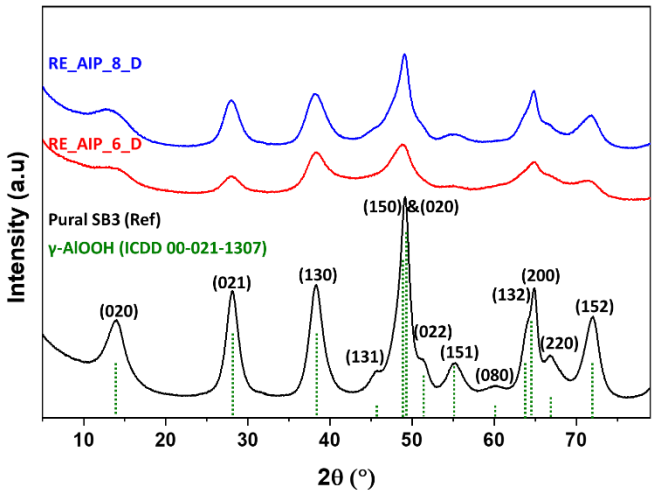


**Fig. 5.** XRD patterns of RE_AlP_8_D and RE_AlP_6_D samples. A commercial boehmite (PuralSB3) and peak indexation from ICDD file are provided for comparison

The Scherrer equation was used to calculate boehmite crystallites dimensions over specific directions (020), (021), and (130) (table 1). RE_AIP_8_D and RE_AIP_6_D have very similar crystallites dimensions of less than 5 nm [67]. Crystallites aspect ratio is calculated from d(020) and d(021). The result is equal or under 0.7 showing that extrudates are made of ultra-small 2D sheet-like nano crystals with moderate aspect ratio [67].

**Table 1 . RE_AIP_6_D and RE_AIP_8_D crystallites length over d(020), d(021), d(130) directions and aspect ratio calculated from d(020), d(021). Taking into consideration that crystallite length evaluation is difficult to evaluate with precision, we added brackets on the last digit of the evaluation.**

| Sample | $d_{(020)}$ (nm) | $d_{(021)}$ (nm) | $d_{(130)}$ (nm) | $d_{(020)}/d_{(021)}$ |
|---|---|---|---|---|
| **RE_AIP_6_D** | 2.(9) | 4.(1) | 3.(9) | 0.7 |
| **RE_AIP_8_D** | 2.(4) | 4.(7) | 3.(7) | 0.5 |

Tettenhorst et al. [68] compared experimental XRD of boehmite powders with calculated one. Their work shows that d(020) reflection 2θ position gives information about crystallite's thickness for

thin nanoparticles. They showed that d(020) reflection slightly shifts below 14.6° for a crystallite thickness inferior to 3 crystal meshes (3.6 nm). Since the position of this peak in our materials is $2\theta_{(020)} < 14.0°$, crystallites thickness can be assumed to be under 3.6 nm, (less than three boehmite sheets in average) which is consistent with thickness calculated by Scherrer equation.

Samples calcined for 4 hours at 540 °C exhibit four main diffraction peaks indexed to the (311), (222), (400) and (440) plans, characteristic of a gamma alumina phase (figure 6).

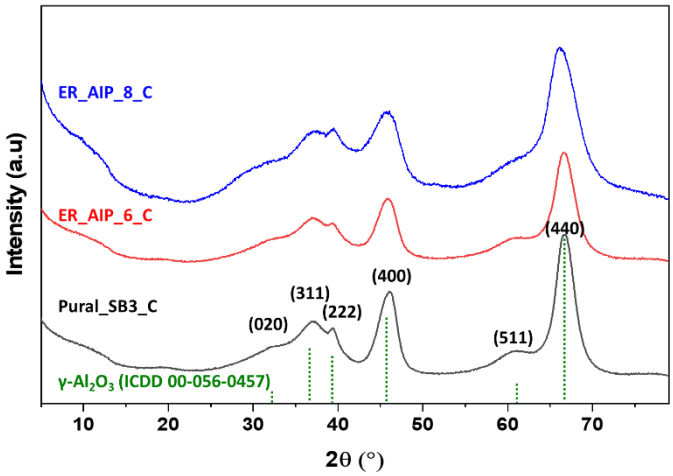


**Fig. 6.** XRD patterns of RE_AIP_8_C and RE_AIP_6_C samples. A commercial gamma alumina obtained by calcining PuralSB3 reference boehmite and peak indexation from ICDD file are provided for comparison

TEM pictures of RE_AIP_8_D sample (cf. figure 7) show that our materials consist of a homogeneous tangle of platelets with an average length of 50 nm (±20). It is possible to observe only few heterogeneous domains of a few hundred nanometers (figure SI.3). From these TEM images, we can hypothesize that the presence of these domains is the signature of partially hydrolyzed AIP grains.

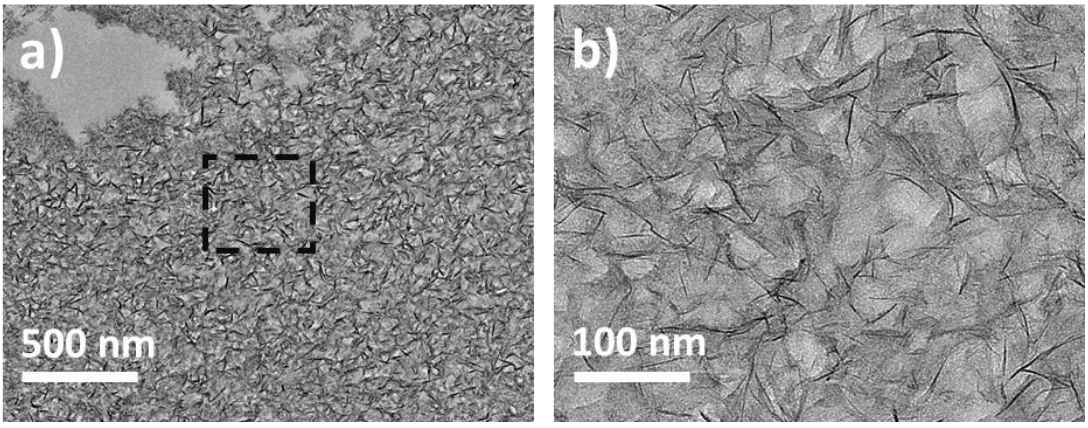


**Fig. 7.** Microtome TEM pictures of RE_AIP_8_ D sample. a) view at a large scale; b) zoom to the black square zone

SEM analyses of calcined extrudates give an overview of the final structure at near macroscopic scale (figure 8). For this analysis, each extrudate was broken in two pieces and the fracture was examined. On the one hand, RE_AIP_6_C extrudates exhibit a heterogeneous composite structure made of grains (size ranging from 1 to 15 micrometers) scattered within a continuous phase. Grains seem poorly cohesive with the continuous phase. Such a microstructure is likely to result from a lack of homogeneity of reactive extrusion/shaping process and can be due either to (i) unreacted alkoxide grains trapped within a partly reacted matrix after extrusion process, and/or (ii) a problem of extrudate compacity resulting from inhomogeneous compression into the dye of the extruder. On the other hand, RE_AIP_8_C images show a homogenous phase, with no large particles (the long fracture line clearly visible on pictures is due to the breaking of the extrudate).

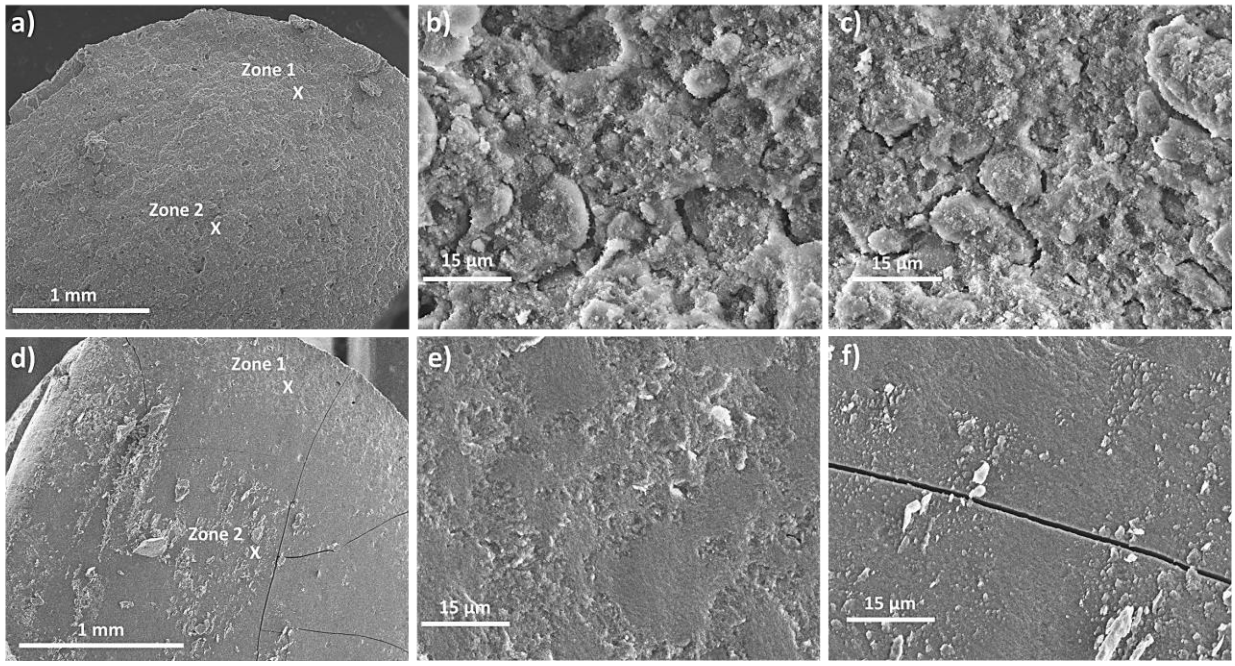


**Fig. 8.** SEM pictures of fractured extrudates: a) RE_AIP_6_C extrudate ; b) RE_AIP_6_C zoom at zone 1 at the edge of extrudate ; c) RE_AIP_6_C zoom at zone 2 in the middle of extrudate ; d) RE_AIP_8_C extrudate e) RE_AIP_8_C zoom at zone 1 at the edge of extrudate ; f) RE_AIP_8_C zoom at zone 2 in the middle of extrudate

Thus, it seems that the mechanical strength of our material is closely related to the phase homogeneity at the micrometer scale, the presence of large particles and holes favoring very probably the propagation of cracks. Whenever calcined extrudates are subjected to a very basic and qualitative mechanical test, crushing between fingers, RE_AIP_8_C is able to resist the pressure without breaking while, RE_AIP_6_C is crushed to powder. To estimate the mechanical strength of RE_AIP_8_C compared to real industrial requirements, we performed a quantitative mechanical test of crushing strength called “side crushing test”. The strongest extrudates broke at 1.14 daN/mm. According to this mechanical test, their integrity is comparable to that of classical industrial extrudates prepared by a conventional kneading/extrusion process [69]. These preliminary results are of very high interest for they prove that extrudates prepared by reactive extrusion are

already close to reaching industrial requirements. The understanding of reactivity mechanisms is likely to help us further improve the cohesion strength of our materials, thus their average value of crushing strength.

**Reaction mechanisms**

From a Sol-Gel chemistry point of view, the reactive medium being essentially granular AIP with few droplets of water, the hydrolysis reaction probably takes place in two steps. In the first step, the extrusion processing intimately mixes the newly added water and AIP grains so that water has little or no diffusion problems to reach the surface of the grains. At AIP grain surface, the hydrolysis starts with a high water/AIP molar ratio (higher than the average rate introduced), resulting in the formation of large aggregates of platelets. Rapidly, hydrolysis leads to the formation of isopropanol which slowly diffuses into AIP grains with the remaining water, creating a hydro-alcoholic front which propagates the hydrolysis reaction towards the center of AIP grains. As a consequence, one can assume that AIP grains are hydrolyzed progressively until they are consumed. Remaining domains observed in figure SI.3 are likely to be the very center of larger AIP grains partially hydrolyzed during the synthesis or/and AIP domains imperfectly mixed with water. From a chemical reaction point of view, the solvent-free hydrolysis and condensation of aluminum alkoxides follows the very specific pathway known for most metal alkoxides that form metal oxoalkoxo polymers of general formula $M^zO_{(\frac{z}{2}-\frac{x}{2}-\frac{y}{2})}\ (OH)_x(OR)_y$ [47,70]. The extra small dimensions of crystallites are characteristic of a massive nucleation process, followed by a very limited growth of crystals due to the very small diffusion coefficient of reactant and product within a highly viscous matrix resulting from the absence of dispersion media (solvent). A second specificity of the solvent-free pathway is that no external heating of the reactant was needed for

producing boehmite, while a heating is most often used to obtain the same crystallographic phase in the presence of a solvent [71]. Yet, in our case, we must highlight that the hydrolysis step is very exothermic, so that the condensation step is in fact running in a hot environment (we monitored 43 °C with the external extruder thermocouple meaning that no external heat is needed for reactive extrusion of our samples). Hence, the result of our experiments is coherent with thermodynamics and literature data highlighting that a warm environment favors the crystallization of boehmite.

**Textural characterization of extrudates**

We analyzed textural properties of dried and calcined extrudates by nitrogen physisorption. Surface area, porous volume, and pore size distribution are listed in table 2. All isotherms (figure SI.4) exhibit hysteresis loops characteristic of wedge-shaped pores [72], which is consistent with TEM observations. RE_IPA_6_D has a specific surface area of 308 $m^2.g^{-1}$, a porous volume of 1.0 $cm^3/g$ and a pore size distribution at desorption centered at 11.2 nm. RE_AIP_8_D extrudates present a higher surface area (391 $m^2.g^{-1}$) and porous volume (1.7 $cm^3.g^{-1}$), as well as a larger pore size distribution (15.2 nm) compared to RE_AIP_6_D. All pore size distributions are asymmetric and broad, extending down to 4 nm. After calcination, RE_AIP_6_C shows an important decrease in surface area, falling down to 228 $m^2.g^{-1}$, while porous volume remained stable at 1.0 $cm^3.g^{-1}$, and mean pore size distribution increased slightly to 12.2 nm. The same trend has been observed for RE_AIP_8_C. It shows a slight decrease in surface area (337 $m^2.g^{-1}$), an increase in pore volume (1.9 $cm^3.g^{-1}$) and larger average pore size (18 nm) (figure SI.5).

**Table 2 . RE_AIP_6_D and RE_AIP_8_D extrudate textural properties. (a) Porous volume was taken at $P/P_0 = 0.99$; (b) pore size distribution was estimated with BJH model at desorption branch.**

| Sample | $S_{BET}$ ($m^2.g^{-1}$) | $Vp^a$ ($cm^3.g^{-1}$) | Pore size[b] (nm) |
|---|---|---|---|

| | | | |
|---|---|---|---|
| **RE_AIP_6_D** | 308 | 1.0 | 11.2 |
| **RE_AIP_6_C** | 228 | 1.0 | 12.2 |
| **RE_AIP_8_D** | 391 | 1.7 | 15.2 |
| **RE_AIP_8_C** | 337 | 1.9 | 18.0 |

Overall, RE_AIP_8_C presents remarkable textural properties, which are comparable or even higher than gamma alumina obtained from salt co-precipitation [73] and complex syntheses [74] (for which no extrudate shaping is reported)**.**

**Catalytic tests**

Calcined extrudates were tested in the gas phase dehydration of ethanol, and compared with a commercial γ-alumina powder of surface area 100 $m^2.g^{-1}$ (commonly used industrially for such reaction) [75]. For comparison, we also used boehmite powders prepared with the same solvent-free reaction but made with a steel anchor in a polypropylene bottle. Resulting materials were then shaped using a usual kneading, peptisation, neutralization and extrusion pathway in order to determine the influence of the shaping process on the catalytic performance. We obtained by this way, two other types of extrudates, KE_ASB_6_C and KE_AIP_5_C of surface area 314 and 302 $m^2.g^{-1}$ respectively (see full characterization in SI.6). This hybrid alternative method (solvent-free boehmite synthesis followed by regular kneading/extrusion) uses more than one device but it is still attractive from a sustainability point of view for it uses no solvent and produces no liquid waste.

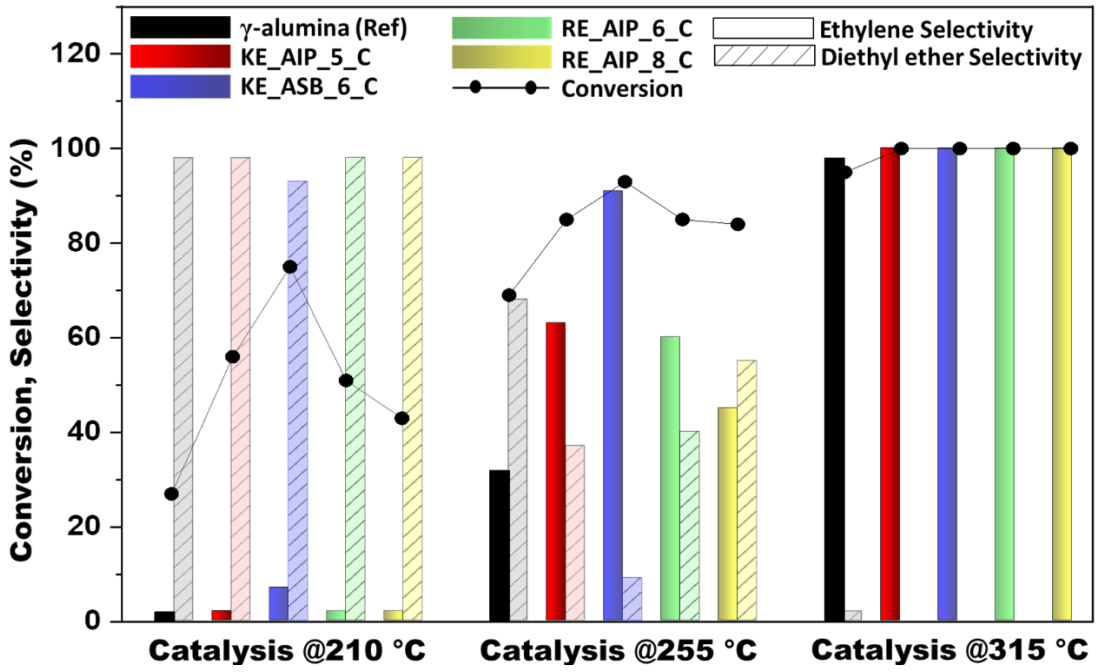


**Fig. 9.** Ethanol dehydration conversion at different temperature catalysis VS Ethylene and Diethyl Ether selectivity

Catalytic tests were made on crushed extrudates. Interestingly, the ethanol conversion is already very significant at 210 °C (higher than 40% for our materials) and even reaches 75% for KE_ASB_6_C sample. As expected, the conversion increases with raising temperature; it is higher than 80% at 255 °C for all materials prepared by solvent-free syntheses and reaches 100% at 315 °C (while the commercial γ-$Al_2O_3$ does not reach full conversion at this temperature). Major products obtained are diethyl ether and ethylene with carbon balance ranging between 95 and 109% (98−103% in majority of experiments). Acetaldehyde and butene (product of ethanol dehydrogenation and ethylene dimerization, respectively) were observed at 255 and 315 °C in minute amounts (< 1%). Higher temperatures favored the production of ethylene in agreement with the reaction thermodynamics and literature [76–79]. From a selectivity point of view, it can be observed that the ethylene selectivity at 255 °C is always higher than 40% and even reaches an

impressive 91% for KE_ASB_6_C sample. This point is to compare with the reference γ-alumina which exhibits only 32% of selectivity at 255 °C. In all cases, the catalysts were very stable during these analyses, similar to other reports on alumina, as it can be seen in figure SI.7 [77,76].

The reference γ-alumina showed similar catalytic behavior to previously reported data on non-shaped commercial alumina and amorphous silica-alumina catalysts [76,80–83]. For example, Phung et al. reported a stepwise increase of ethanol conversion from 2−21% to 72−98% when changing temperatures from 200 to 300 °C at WHSV = 1.43 $h^{-1}$ over commercial alumina catalysts prepared by various methods (flame hydrolysis; precipitation of Al salts; synthesized from Al alkoxides). Commercial silica-alumina displayed similar catalytic behavior [76,82]. The materials produced by solvent-free synthesis and shaped as extrudates after kneeding-extrusion or directly by reactive extrusion exhibited comparable or better dehydration activity. More globally, a simple selectivity and conversion comparison with results of the literature showed that our results are comparable with those of pure inorganic and hybrid aluminosilicate catalysts obtained by an advanced non-hydrolytic sol-gel method (ethanol conversion~85%, selectivity to ethylene 60−80% at 240 °C and identical WHSV) [59,80,84]. The HZSM-5 molecular sieve containing strong Brønsted acid sites showed a higher catalytic activity (ethanol conversion~90%, selectivity to ethylene 90% at 240 °C and WHSV = 17.5 $h^{-1}$) [80], however it suffers from rapid deactivation by coking [80,81]. Although a precise performance evaluation of our samples would need a dedicated study at low conversion (less than 20%) and acidity measurement tests, the materials presented herein display a high potential for catalytic applications, not only from the point of view of catalytic performance, but also from a sustainability point of view as discussed in the following section.

**Atoms and energy metrics**

We made an attempt to compare the one-step reactive extrusion approach with a boehmite synthesis approach using precipitation at high concentration of reactants (which is representative of industrial reality) [34]. In this section, we calculated atom and energy consumptions, estimated E-factor (total mass of waste divided by the produced mass of catalyst) and space time yield of production (the mass of final product obtained per cubic meter of reactor in one day). We highlight here that the E-factor usually does not consider water in its calculation. The pertinence of this point can be debated for all liquid wastes dissolved in water are not easily eliminated and water recycling costs time and energy. Also, considering that water rarefaction is considered by United Nations as one of the seventeen challenges to solve for the coming century, we decided to consider water and thus also calculate what is commonly referred to as the "complete E-factor" (cE-factor) [14]. We compared three scenarios considering only the preparation of dry boehmite. For this comparison, we excluded calcination for it is the same for materials prepared by reactive extrusion and precipitation. We highlight that, while reactive extrusion integrates a shaping step, the precipitation method requires additional kneading and shaping steps (i.e. two more tools with their energy consumption and longer preparation time). These additional costs were not included in the energetic comparison presented below.

The first scenario is the conventional synthesis method in which aluminum salts are precipitated in water, then filtered, washed and dried. In that case, we considered the use of 0.75 $mol.l^{-1}$ of aluminum salt in water and two possible precipitation temperatures, 30 and 85°C. For washing, we considered that three times the reaction volume of solvent at ambient temperature is required (this step is usually not described in literature but from salt counterions dilution calculations, three washings are likely to be a minimum). The second scenario is the equivalent of the first one, pushed at its theoretical limit, that is, we consider that the aqueous solution of aluminum nitrate salt is

saturated before reaction. This was calculated for determining the theoretical limit of the precipitation approach. The third scenario is the case of the reactive extrusion presented herein, requiring no energy input for heating (the exothermicity of the reaction is enough for promoting boehmite crystallization, as demonstrated above).

The energy consumption of devices is not included in the calculations. Similarly it is considered that precipitation reactors are perfectly isolated from a thermal point of view. We considered only the energy required for the chemical reaction, and washing (heating of water). The powder drying energy consumption was calculated by considering only the vaporization enthalpy of remaining solvent (the wet cake of boehmite typically contains in between 84% and 93% of water by weight before drying [42,43], and isopropanol for reactive extrusion). We summarized the comparison in the table 3.

**Table 3 . Minimal atom and energy consumption, E-Factor and cE-factor calculated for a conventional precipitation, a fictive ideal precipitation, and for the reactive extrusion, the production of one kg of AlOOH. a) Precipitation temperature is 30 °C; b) precipitation temperature is 85 °C; c) hydration water of the salt was removed for this calculation**

| | Reference precipitation | Theoretical limit of precipitation | Reactive extrusion |
|---|---|---|---|
| **ATOMS** | | | |
| Water (kg) | 102.4 | 41.9 | 2.39 |
| Aluminium salts (mol) | 16.6 | 16.6 | - |
| Aluminium alkoxide (mol) | | | 16.6 |
| $NH_4OH$ (kg) | 1.4 | 1.4 | - |
| **ENERGY** | | | |
| Solvent heating (MJ) | 4.3[a] to 27.8[b] | 1.7[a] to 11.4[b] | - |
| Vaporization (MJ) | 21.9 | 21.9 | 1.9 |
| **E-FACTOR** | 7.5[c] | 7.5[c] | 3.4 |
| **cE-FACTOR** | 110.0 | 49.5 | 5.8 |

The comparison of water consumption between precipitation and solvent-free reactive extrusion methods highlights immediately the huge advantage of reactive extrusion which simply does not use any solvent. E-factor calculation (more representative of atom consumption at the industrial scale) is more than two times higher for precipitation method if we do not consider water. Yet, using chemical grade water (either purified or recycled) has a cost. The more realistic comparison based on the cE-factors yields a value of 110, that is, nearly 19 times higher than the reactive extrusion method. When compared with the theoretical limit of the precipitation method (that is starting from a salt-saturated solution), the cE-factor of reactive extrusion is still 8 times lower, highlighting the very significant sustainability gain that can be achieved by using reactive extrusion processing. From an energy consumption point of view, the precipitation method consumes energy for heating the precipitation solution and evaporating the remaining solvent from the final boehmite. Reactive extrusion consumes 12 times less energy. This calculation does not take in consideration the energetic consumption of devices used for mixing, kneading, filtering and washing of precipitation approach so that the advantage of reactive extrusion is actually underestimated.

Altogether, from an industrial point of view, the Space Time Yield (STY) is another useful indicator. Intrinsically, reactive extrusion using mass reaction with no solvent reaches very high STY. In the present case, the calculation can be performed in two ways. If one considers that the volume of the twin screw of the extruder is a part of the volume of the reactor, the STY of our process is 11525 $kg.m^{-3}.day^{-1}$. If one considers that the volume of the used reactor is the volume of reactants only, STY is five time higher. We did not find in literature any proper estimation of STY for standard manufacture of boehmite by precipitation. Yet, we can compare with other

materials prepared by precipitation such as MOFs. The optimized BASF production of aluminium fumarate is amongst the best ever reported in literature with a STY of only 3600 $kg.m^{-3}.day^{-1}$ [85].

Finally, we did not discuss the production cost for it depends very much on the industrial environment, manpower cost, investment cost, maintenance cost and chemical reactant cost. The latter is difficult to estimate at industrial scale for it depends on negotiations. While Al alkoxides are significantly more expensive than the chlorides or nitrates counterparts, we can very probably balance the reactants cost difference with the huge gains in energy, manpower and maintenance costs. Continuous reactive extrusion processing, using only one device from the chemical reaction to the final shaping of the catalyst, is likely a realistic alternative to batch precipitation method using several devices with a global improved environmental footprint.

## 5. Conclusion

To summarize, we presented a new integrated method for the green synthesis and shaping of high surface area boehmite supports. The obtained materials are successfully prepared in one step via a solvent-free pathway using aluminium alkoxides that requires no sacrificial organic pore generating agent such as surfactant or polymer, no washing, no filtration, and produces no liquid waste. Upon calcination high surface area γ-alumina extrudates are readily obtained. Thus, this solvent-free synthesis strategy can be easily implemented for the industrial production of heterogeneous catalysts or supports. We proved that the shaped γ-alumina materials prepared through reactive extrusion exhibit high ethanol dehydration catalytic properties, competing with similar materials. The decisive advantage of this innovative method is the drastic intensification of the production process, featuring sustainability metrics (atom economy, energy consumption, E-factor, cE-factor) that are outstanding, as compared to those of the conventional precipitation method. Indeed, by comparison with a standard production method – even if using highly

concentrated aqueous salt solutions – the reactive extrusion process uses one extruder for replacing several devices (used for mixing, filtering, washing, and kneading), and it completely eliminates all filtration and, if salt precursors are used, washing steps. Concomitantly, we replace a batch production process by a continuous production process allowing removing the need of heating large volume of solvents (the hydrolysis of reactant produces enough energy for boehmite synthesis).

As this last aspect also allows saving a lot of atom, energy, and manpower, we do believe that the strategy presented here paves the way to the sustainable industrial production of such nanomaterials. Such one step-one tool process opens new interesting ways for shaping porous materials synthesis since it may subsequently be reproduced for many other oxides as far as alkoxides are available. Due to the great versatility of the process, the preparation of more complex materials such as mixed oxides or metal-supported oxide catalysts can also be envisaged.

AUTHOR INFORMATION


### Corresponding Author

* cedric.boissie@sorbonne-universite.fr.

### Present Addresses

†If an author's address is different than the one given in the affiliation line, this information may be included here.


### Author Contributions

‡ Pierre-Igor Dassie performed materials synthesis, characterizations, bibliographic studies and manuscript writing

‡ Ryma Haddad performed materials synthesis, characterizations, bibliographic studies and manuscript writing

Maud Lenez performed materials synthesis and characterizations

Alexandra Chaumonnot performed conceptual conception, student management, data interpretation and manuscript writing

Malika Boualleg performed conceptual conception, student management, data interpretation and manuscript writing

Patrick Legriel performed electron microscopy experiments

Ales Styskalik performed catalytic tests experiments and data treatments

Bernard Haye performed microtome cut of sample

Mohamed Selmane performed XRD analyses and modelizations.

Damien P. Debecker performed catalytic studies conception and interpretations, management, and manuscript writing

Clement Sanchez performed conceptual conception, data interpretation and manuscript writing

Corinne Chaneac performed conceptual conception, student management, data interpretation and manuscript writing

Cedric Boissiere performed conceptual conception, student management, data interpretation and manuscript writing

## Funding Sources

This work was supported by IFPEN and by ED397 Doctoral School Materials Physics/Chemistry of Sorbonne University.

REFERENCES

(1) *Heterogeneous Catalysis for Energy Applications*; 2020. https://doi.org/10.1039/9781788019576.
(2) Ross, J. R. H. Chapter 12 - Catalytic Reactions Involving Syngas, Hydrogen, or Carbon Monoxide for the Production of Intermediates and Chemicals. In *Contemporary Catalysis*; Ross, J. R. H., Ed.; Elsevier: Amsterdam, 2019; pp 273–290. https://doi.org/10.1016/B978-0-444-63474-0.00012-6.
(3) *Environmental Catalysis*; Grassian, V. H., Ed.; CRC Press: Boca Raton, 2005. https://doi.org/10.1201/9781420027679.
(4) Morales-Torres, S.; Pastrana-Martínez, L. M.; Maldonado-Hódar, F. J. Carbon Nanomaterials for Air and Water Remediation. In *Nanostructured Catalysts for Environmental Applications*; Piumetti, M., Bensaid, S., Eds.; Springer International Publishing: Cham, 2021; pp 331–365. https://doi.org/10.1007/978-3-030-58934-9_12.
(5) Marin Figueredo, M. J.; Piumetti, M.; Bensaid, S.; Fino, D.; Nunzio, R. Catalytic Oxidation of Volatile Organic Compounds over Porous Manganese Oxides Prepared via Sol-Gel Method. In *Nanostructured Catalysts for Environmental Applications*; Piumetti, M.,

Bensaid, S., Eds.; Springer International Publishing: Cham, 2021; pp 59–78. https://doi.org/10.1007/978-3-030-58934-9_2.
(6) Ndolomingo, M. J.; Bingwa, N.; Meijboom, R. Review of Supported Metal Nanoparticles: Synthesis Methodologies, Advantages and Application as Catalysts. *J. Mater. Sci.* **2020**, *55* (15), 6195–6241. https://doi.org/10.1007/s10853-020-04415-x.
(7) Ferlin, F.; Santoro, S.; Ackermann, L.; Vaccaro, L. Heterogeneous C–H Alkenylations in Continuous-Flow: Oxidative Palladium-Catalysis in a Biomass-Derived Reaction Medium. *Green Chem.* **2017**, *19* (11), 2510–2514. https://doi.org/10.1039/C7GC01103B.
(8) Irfan, M.; Glasnov, T. N.; Kappe, C. O. Heterogeneous Catalytic Hydrogenation Reactions in Continuous-Flow Reactors. *ChemSusChem* **2011**, *4* (3), 300–316. https://doi.org/10.1002/cssc.201000354.
(9) Ross, J. R. H. Chapter 7 - Large-Scale Catalytic Reactors. In *Heterogeneous Catalysis*; Ross, J. R. H., Ed.; Elsevier: Amsterdam, 2012; pp 143–169. https://doi.org/10.1016/B978-0-444-53363-0.10007-6.
(10) Touati, H.; Valange, S.; Reinholdt, M.; Batiot-Dupeyrat, C.; Clacens, J.-M.; Tatibouët, J.-M. Low Temperature Catalytic Oxidation of Ethanol Using Ozone over Manganese Oxide-Based Catalysts in Powdered and Monolithic Forms. *Catalysts* **2022**, *12* (2), 172. https://doi.org/10.3390/catal12020172.
(11) Lakiss, L.; Gilson, J.-P.; Valtchev, V.; Mintova, S.; Vicente, A.; Vimont, A.; Bedard, R.; Abdo, S.; Bricker, J. Zeolites in a Good Shape: Catalyst Forming by Extrusion Modifies Their Performances. *Microporous Mesoporous Mater.* **2020**, *299*, 110114. https://doi.org/10.1016/j.micromeso.2020.110114.
(12) Middelkoop, V.; Vamvakeros, A.; de Wit, D.; Jacques, S. D. M.; Danaci, S.; Jacquot, C.; de Vos, Y.; Matras, D.; Price, S. W. T.; Beale, A. M. 3D Printed Ni/Al2O3 Based Catalysts for CO2 Methanation - a Comparative and Operando XRD-CT Study. *J. CO2 Util.* **2019**, *33*, 478–487. https://doi.org/10.1016/j.jcou.2019.07.013.
(13) Alimi, O. A.; Ncongwane, T. B.; Meijboom, R. Design and Fabrication of a Monolith Catalyst for Continuous Flow Epoxidation of Styrene in Polypropylene Printed Flow Reactor. *Chem. Eng. Res. Des.* **2020**, *159*, 395–409. https://doi.org/10.1016/j.cherd.2020.04.025.
(14) Debecker, D. P.; Kuok (Mimi) Hii, K.; Moores, A.; Rossi, L. M.; Sels, B.; Allen, D. T.; Subramaniam, B. Shaping Effective Practices for Incorporating Sustainability Assessment in Manuscripts Submitted to ACS Sustainable Chemistry & Engineering: Catalysis and Catalytic Processes. *ACS Sustain. Chem. Eng.* **2021**, *9* (14), 4936–4940. https://doi.org/10.1021/acssuschemeng.1c02070.
(15) Vora, B. V. Development of Dehydrogenation Catalysts and Processes. *Top. Catal.* **2012**, *55* (19), 1297–1308. https://doi.org/10.1007/s11244-012-9917-9.
(16) Abdulrasheed, A.; Jalil, A. A.; Gambo, Y.; Ibrahim, M.; Hambali, H. U.; Shahul Hamid, M. Y. A Review on Catalyst Development for Dry Reforming of Methane to Syngas: Recent Advances. *Renew. Sustain. Energy Rev.* **2019**, *108*, 175–193. https://doi.org/10.1016/j.rser.2019.03.054.
(17) Bagnato, G.; Sanna, A.; Paone, E.; Catizzone, E. Recent Catalytic Advances in Hydrotreatment Processes of Pyrolysis Bio-Oil. *Catalysts* **2021**, *11* (2), 157. https://doi.org/10.3390/catal11020157.
(18) Feng, F.; Shang, Z.; Wang, L.; Zhang, X.; Liang, X.; Wang, Q. Structure-Sensitive Hydro-Conversion of Oleic Acid to Aviation-Fuel-Range-Alkanes over Alumina-Supported Nickel

Catalyst. *Catal. Commun.* **2020**, *134*, 105842. https://doi.org/10.1016/j.catcom.2019.105842.
(19) Hattori, H.; Ono, Y. 4 - Catalysts and Catalysis for Acid–Base Reactions. In *Metal Oxides in Heterogeneous Catalysis*; Védrine, J. C., Ed.; Metal Oxides; Elsevier, 2018; pp 133–209. https://doi.org/10.1016/B978-0-12-811631-9.00004-1.
(20) Wischert, R.; Laurent, P.; Copéret, C.; Delbecq, F.; Sautet, P. γ-Alumina: The Essential and Unexpected Role of Water for the Structure, Stability, and Reactivity of "Defect" Sites. *J. Am. Chem. Soc.* **2012**, *134* (35), 14430–14449. https://doi.org/10.1021/ja3042383.
(21) Euzen, P.; Raybaud, P.; Krokidis, X.; Toulhoat, H.; Le Loarer, J.-L.; Jolivet, J.-P.; Froidefond, C. Alumina. In *Handbook of Porous Solids*; John Wiley & Sons, Ltd, 2002; pp 1591–1677. https://doi.org/10.1002/9783527618286.ch23b.
(22) Lippens, B. C. Structure and Texture of Aluminas. **1961**.
(23) Valette, A. Amélioration Des Propriétés Texturales de l'alumine Par Le Contrôle de l'état d'agrégation de Bâtonnets. These de doctorat, Sorbonne université, 2019. https://www.theses.fr/2019SORUS395 (accessed 2023-01-31).
(24) Hritz, G. G.; Leach, B. E.; Royer, D. J. ALUMINUM OXYDE EXTRUDATE AND PROCESS FOR ITS MANUFACTURING. DE2237861A1, February 22, 1973. https://patents.google.com/patent/DE2237861A1/en (accessed 2022-10-14).
(25) Brink, P. J. V. D.; Dogterom, R. J.; Mesters, C. M. A. M. Method of Manufacturing a Catalyst. US7582588B2, September 1, 2009. https://patents.google.com/patent/US7582588B2/en?oq=V.D.+Brink%2c+Method+of+manufacturing+a+catalyst%2c+US+patent+7582588%2c+(2009) (accessed 2022-10-14).
(26) Yoldas, B. E. Hydrolysis of Aluminium Alkoxides and Bayerite Conversion. *J. Appl. Chem. Biotechnol.* **1973**, *23* (11), 803–809. https://doi.org/10.1002/jctb.5020231103.
(27) Adschiri, T.; Kanazawa, K.; Arai, K. Rapid and Continuous Hydrothermal Synthesis of Boehmite Particles in Subcritical and Supercritical Water. *J. Am. Ceram. Soc.* **1992**, *75* (9), 2615–2618. https://doi.org/10.1111/j.1151-2916.1992.tb05625.x.
(28) Okada, K.; Nagashima, T.; Kameshima, Y.; Yasumori, A.; Tsukada, T. Relationship between Formation Conditions, Properties, and Crystallite Size of Boehmite. *J. Colloid Interface Sci.* **2002**, *253* (2), 308–314. https://doi.org/10.1006/jcis.2002.8535.
(29) Kotanigawa, T.; Yamamoto, M.; Utiyama, M.; Hattori, H.; Tanabe, K. The Influence of Preparation Methods on the Pore Structure of Alumina. *Appl. Catal.* **1981**, *1* (3), 185–200. https://doi.org/10.1016/0166-9834(81)80006-1.
(30) Toledo, R. R.; Santoyo, V. R.; Sánchez, C. D. M.; Rosales, M. M. Effect of Aluminum Precursor on Physicochemical Properties of Al2O3 by Hydrolysis/Precipitation Method. *Nova Sci.* **2018**, *10* (20), 83–99. https://doi.org/10.21640/ns.v10i20.1217.
(31) Ramanathan, S.; Roy, S. K.; Bhat, R.; Upadhyaya, D. D.; Biswas, A. R. Alumina Powders from Aluminium Nitrate-Urea and Aluminium Sulphate-Urea Reactions — The Role of the Precursor Anion and Process Conditions on Characteristics. *Ceram. Int.* **1997**, *23* (1), 45–53. https://doi.org/10.1016/0272-8842(95)00139-5.
(32) Brusasco, R.; Gnassi, J.; Tatian, C.; Baglio, J.; Dwight, K.; Wold, A. Preparation and Characterization of Fibrillar Boehmite and γ-Al2O3. *Mater. Res. Bull.* **1984**, *19* (11), 1489–1496. https://doi.org/10.1016/0025-5408(84)90263-0.
(33) Morgado, E.; Lam, Y. L.; Nazar, L. F. Formation of Peptizable Boehmites by Hydrolysis of Aluminum Nitrate in Aqueous Solution. *J. Colloid Interface Sci.* **1997**, *188* (2), 257–269. https://doi.org/10.1006/jcis.1997.4780.

(34) Karouia, F.; Boualleg, M.; Digne, M.; Alphonse, P. Control of the Textural Properties of Nanocrystalline Boehmite (γ-AlOOH) Regarding Its Peptization Ability. *Powder Technol.* **2013**, *237*, 602–609. https://doi.org/10.1016/j.powtec.2012.12.054.
(35) Ozkan, S.; Gevgilili, H.; Kalyon, D. M.; Kowalczyk, J.; Mezger, M. Twin-Screw Extrusion of Nano-Alumina–Based Simulants of Energetic Formulations Involving Gel-Based Binders. *J. Energ. Mater.* **2007**, *25* (3), 173–201. https://doi.org/10.1080/07370650701399320.
(36) Debecker, D. P.; Boissière, C.; Laurent, G.; Huet, S.; Eliaers, P.; Sanchez, C.; Backov, R. First Acidic Macro-Mesocellular Aluminosilicate Monolithic Foams "SiAl(HIPE)" and Their Catalytic Properties. *Chem. Commun.* **2015**, *51* (74), 14018–14021. https://doi.org/10.1039/C5CC05328E.
(37) Devyatkov, S. Yu.; Zinnurova, A. Al.; Aho, A.; Kronlund, D.; Peltonen, J.; Kuzichkin, N. V.; Lisitsyn, N. V.; Murzin, D. Yu. Shaping of Sulfated Zirconia Catalysts by Extrusion: Understanding the Role of Binders. *Ind. Eng. Chem. Res.* **2016**, *55* (23), 6595–6606. https://doi.org/10.1021/acs.iecr.6b00820.
(38) Murzin, D. Y. *Engineering Catalysis*; De Gruyter, 2020. https://doi.org/10.1515/9783110614435.
(39) Digne, M.; Sautet, P.; Raybaud, P.; Toulhoat, H.; Artacho, E. Structure and Stability of Aluminum Hydroxides: A Theoretical Study. *J. Phys. Chem. B* **2002**, *106* (20), 5155–5162. https://doi.org/10.1021/jp014182a.
(40) Smith, S. J.; Amin, S.; Woodfield, B. F.; Boerio-Goates, J.; Campbell, B. J. Phase Progression of γ-Al2O3 Nanoparticles Synthesized in a Solvent-Deficient Environment. *Inorg. Chem.* **2013**, *52* (8), 4411–4423. https://doi.org/10.1021/ic302593f.
(41) Le Page, J. F. *Applied Heterogeneous Ca...*; Editions OPHRYS, 1987.
(42) Lafficher, R. Nouveau procédé de précipitation pour la synthèse d'alumine. phdthesis, Université de Lyon, 2016. https://tel.archives-ouvertes.fr/tel-01425446 (accessed 2022-07-22).
(43) Lafficher, R.; Digne, M.; Salvatori, F.; Boualleg, M.; Colson, D.; Puel, F. Ammonium Aluminium Carbonate Hydroxide NH4Al(OH)2CO3 as an Alternative Route for Alumina Preparation: Comparison with the Classical Boehmite Precursor. *Powder Technol.* **2017**, *320*, 565–573. https://doi.org/10.1016/j.powtec.2017.07.080.
(44) Manas-Zloczower, I. *Mixing and Compounding of Polymers: Theory and Practice*; Hanser, 2009.
(45) Lambla, M. Reactive Extrusion. In *Rheological Fundamentals of Polymer Processing*; Covas, J. A., Agassant, J. F., Diogo, A. C., Vlachopoulos, J., Walters, K., Eds.; NATO ASI Series; Springer Netherlands: Dordrecht, 1995; pp 437–454. https://doi.org/10.1007/978-94-015-8571-2_20.
(46) Crawford, D.; Casaban, J.; Haydon, R.; Giri, N.; McNally, T.; James, S. L. Synthesis by Extrusion: Continuous, Large-Scale Preparation of MOFs Using Little or No Solvent. *Chem. Sci.* **2015**, *6* (3), 1645–1649. https://doi.org/10.1039/C4SC03217A.
(47) Livage, J.; Henry, M.; Sanchez, C. Sol-Gel Chemistry of Transition Metal Oxides. *Prog. Solid State Chem.* **1988**, *18* (4), 259–341. https://doi.org/10.1016/0079-6786(88)90005-2.
(48) Nguefack, M.; Popa, A. F.; Rossignol, S.; Kappenstein, C. Preparation of Alumina through a Sol–Gel Process. Synthesis, Characterization, Thermal Evolution and Model of Intermediate Boehmite. *Phys. Chem. Chem. Phys.* **2003**, *5* (19), 4279–4289. https://doi.org/10.1039/B306170A.

(49) Lueangchaichaweng, W.; Singh, B.; Mandelli, D.; Carvalho, W. A.; Fiorilli, S.; Pescarmona, P. P. High Surface Area, Nanostructured Boehmite and Alumina Catalysts: Synthesis and Application in the Sustainable Epoxidation of Alkenes. *Appl. Catal. Gen.* **2019**, *571*, 180–187. https://doi.org/10.1016/j.apcata.2018.12.017.
(50) May, M.; Navarrete, J.; Asomoza, M.; Gomez, R. Tailored Mesoporous Alumina Prepared from Different Aluminum Alkoxide Precursors. *J. Porous Mater.* **2007**, *14* (2), 159–164. https://doi.org/10.1007/s10934-006-9020-3.
(51) Rajaeiyan, A.; Bagheri-Mohagheghi, M. M. Comparison of Sol-Gel and Co-Precipitation Methods on the Structural Properties and Phase Transformation of γ and α-Al2O3 Nanoparticles. *Adv. Manuf.* **2013**, *1* (2), 176–182. https://doi.org/10.1007/s40436-013-0018-1.
(52) Huang, B.; Bartholomew, C. H.; Smith, S. J.; Woodfield, B. F. Facile Solvent-Deficient Synthesis of Mesoporous γ-Alumina with Controlled Pore Structures. *Microporous Mesoporous Mater.* **2013**, *165*, 70–78. https://doi.org/10.1016/j.micromeso.2012.07.052.
(53) Huang, B.; Bartholomew, C. H.; Woodfield, B. F. Facile Structure-Controlled Synthesis of Mesoporous γ-Alumina: Effects of Alcohols in Precursor Formation and Calcination. *Microporous Mesoporous Mater.* **2013**, *177*, 37–46. https://doi.org/10.1016/j.micromeso.2013.04.013.
(54) Huang, B.; Bartholomew, C. H.; Woodfield, B. F. Facile Synthesis of Mesoporous γ-Alumina with Tunable Pore Size: The Effects of Water to Aluminum Molar Ratio in Hydrolysis of Aluminum Alkoxides. *Microporous Mesoporous Mater.* **2014**, *183*, 37–47. https://doi.org/10.1016/j.micromeso.2013.09.007.
(55) Smith, S. J.; Huang, B.; Liu, S.; Liu, Q.; Olsen, R. E.; Boerio-Goates, J.; Woodfield, B. F. Synthesis of Metal Oxide Nanoparticles via a Robust "Solvent-Deficient" Method. *Nanoscale* **2014**, *7* (1), 144–156. https://doi.org/10.1039/C4NR04964K.
(56) Oh, J.; Bathula, H. B.; Park, J. H.; Suh, Y.-W. A Sustainable Mesoporous Palladium-Alumina Catalyst for Efficient Hydrogen Release from N-Heterocyclic Liquid Organic Hydrogen Carriers. *Commun. Chem.* **2019**, *2* (1), 1–10. https://doi.org/10.1038/s42004-019-0167-7.
(57) Kore, R. M.; Lokhande, B. J. A Robust Solvent Deficient Route Synthesis of Mesoporous Fe2O3 Nanoparticles as Supercapacitor Electrode Material with Improved Capacitive Performance. *J. Alloys Compd.* **2017**, *725*, 129–138. https://doi.org/10.1016/j.jallcom.2017.07.145.
(58) Woodfield, B. F.; Liu, S.; Boerio-Goates, J.; Liu, Q.; Smith, S. J. Preparation of Uniform Nanoparticles of Ultra-High Purity Metal Oxides, Mixed Metal Oxides, Metals, and Metal Alloys. US8211388B2, July 3, 2012. https://patents.google.com/patent/US8211388B2/en?oq=US8211388 (accessed 2022-03-08).
(59) Styskalik, A.; Vykoukal, V.; Fusaro, L.; Aprile, C.; Debecker, D. P. Mildly Acidic Aluminosilicate Catalysts for Stable Performance in Ethanol Dehydration. *Appl. Catal. B Environ.* **2020**, *271*, 118926. https://doi.org/10.1016/j.apcatb.2020.118926.
(60) Cross, A. D. *An Introduction to Practical Infra-Red Spectroscopy*; Butterworths, 1964.
(61) Smith, B. The Infrared Spectra of Polymers V: Epoxies. **2022**.
(62) Battaglin, F. A. D.; Hosokawa, R. S.; Cruz, N. C. da; Caseli, L.; Rangel, E. C.; Silva, T. F. da; Tabacniks, M. H. Innovative Low Temperature Plasma Approach for Deposition of

Alumina Films. *Mater. Res.* **2014**, *17*, 1410–1419. https://doi.org/10.1590/1516-1439.283514.
(63) Kiss, A. B.; Keresztury, G.; Farkas, L. Raman and i.r. Spectra and Structure of Boehmite (γ-AlOOH). Evidence for the Recently Discarded D172h Space Group. *Spectrochim. Acta Part Mol. Spectrosc.* **1980**, *36* (7), 653–658. https://doi.org/10.1016/0584-8539(80)80024-9.
(64) Morterra, C.; Magnacca, G. A Case Study: Surface Chemistry and Surface Structure of Catalytic Aluminas, as Studied by Vibrational Spectroscopy of Adsorbed Species. *Catal. Today* **1996**, *27* (3), 497–532. https://doi.org/10.1016/0920-5861(95)00163-8.
(65) Barraclough, C. G.; Bradley, D. C.; Lewis, J.; Thomas, I. M. 510. The Infrared Spectra of Some Metal Alkoxides, Trialkylsilyloxides, and Related Silanols. *J. Chem. Soc. Resumed* **1961**, No. 0, 2601–2605. https://doi.org/10.1039/JR9610002601.
(66) Turova, N. Ya.; Kozunov, V. A.; Yanovskii, A. I.; Bokii, N. G.; Struchkov, Yu. T.; Tarnopol'skii, B. L. Physico-Chemical and Structural Investigation of Aluminium Isopropoxide. *J. Inorg. Nucl. Chem.* **1979**, *41* (1), 5–11. https://doi.org/10.1016/0022-1902(79)80384-X.
(67) Chiche, D.; Digne, M.; Revel, R.; Chanéac, C.; Jolivet, J.-P. Accurate Determination of Oxide Nanoparticle Size and Shape Based on X-Ray Powder Pattern Simulation: Application to Boehmite AlOOH. *J. Phys. Chem. C* **2008**, *112* (23), 8524–8533. https://doi.org/10.1021/jp710664h.
(68) Tettenhorst, R. T.; Corbató, C. E. Comparison of Experimental and Calculated X-Ray Powder Diffraction Data for Boehmite. *Clays Clay Miner.* **1988**, *36* (2), 181–183. https://doi.org/10.1346/CCMN.1988.0360213.
(69) Staub, D.; Meille, S.; Corre, V. L.; Chevalier, J.; Rouleau, L. Revisiting the Side Crushing Test Using the Three-Point Bending Test for the Strength Measurement of Catalyst Supports. *Oil Gas Sci. Technol. – Rev. D'IFP Energ. Nouv.* **2015**, *70* (3), 475–486. https://doi.org/10.2516/ogst/2013214.
(70) Blanchard, J.; Ribot, F.; Sanchez, C.; Bellot, P.-V.; Trokiner, A. Structural Characterization of Titanium-Oxo-Polymers Synthesized in the Presence of Protons or Complexing Ligands as Inhibitors. *J. Non-Cryst. Solids* **2000**, *265* (1), 83–97. https://doi.org/10.1016/S0022-3093(99)00885-6.
(71) Stiles, A. B. *Catalyst Supports and Supported Catalysts: Theoretical and Applied Concepts*; Butterworths: Boston, 1987.
(72) Sing, K. S. W. Reporting Physisorption Data for Gas/Solid Systems with Special Reference to the Determination of Surface Area and Porosity (Recommendations 1984). *Pure Appl. Chem.* **1985**, *57* (4), 603–619. https://doi.org/10.1351/pac198557040603.
(73) Okada, K.; Nagashima, T.; Kameshima, Y.; Yasumori, A. Effect of Crystallite Size on the Thermal Phase Change and Porous Properties of Boehmite. *J. Colloid Interface Sci.* **2002**, *248* (1), 111–115. https://doi.org/10.1006/jcis.2001.8183.
(74) Milanović, M.; Obrenović, Z.; Stijepović, I.; Nikolić, L. M. Nanocrystalline Boehmite Obtained at Room Temperature. *Ceram. Int.* **2018**, *44* (11), 12917–12920. https://doi.org/10.1016/j.ceramint.2018.04.103.
(75) Mohsenzadeh, A.; Zamani, A.; Taherzadeh, M. J. Bioethylene Production from Ethanol: A Review and Techno-Economical Evaluation. *ChemBioEng Rev.* **2017**, *4* (2), 75–91. https://doi.org/10.1002/cben.201600025.

(76) Phung, T. K.; Proietti Hernández, L.; Lagazzo, A.; Busca, G. Dehydration of Ethanol over Zeolites, Silica Alumina and Alumina: Lewis Acidity, Brønsted Acidity and Confinement Effects. *Appl. Catal. Gen.* **2015**, *493*, 77–89. https://doi.org/10.1016/j.apcata.2014.12.047.
(77) Zhang, M.; Yu, Y. Dehydration of Ethanol to Ethylene. *Ind. Eng. Chem. Res.* **2013**, *52* (28), 9505–9514. https://doi.org/10.1021/ie401157c.
(78) Fan, D.; Dai, D.-J.; Wu, H.-S. Ethylene Formation by Catalytic Dehydration of Ethanol with Industrial Considerations. *Materials* **2013**, *6* (1), 101–115. https://doi.org/10.3390/ma6010101.
(79) Angelici, C.; Weckhuysen, B. M.; Bruijnincx, P. C. A. Chemocatalytic Conversion of Ethanol into Butadiene and Other Bulk Chemicals. *ChemSusChem* **2013**, *6* (9), 1595–1614. https://doi.org/10.1002/cssc.201300214.
(80) Styskalik, A.; Kordoghli, I.; Poleunis, C.; Delcorte, A.; Moravec, Z.; Simonikova, L.; Kanicky, V.; Aprile, C.; Fusaro, L.; Debecker, D. P. Hybrid Mesoporous Aluminosilicate Catalysts Obtained by Non-Hydrolytic Sol–Gel for Ethanol Dehydration. *J. Mater. Chem. A* **2020**, *8* (44), 23526–23542. https://doi.org/10.1039/D0TA07016E.
(81) Zhang, X.; Wang, R.; Yang, X.; Zhang, F. Comparison of Four Catalysts in the Catalytic Dehydration of Ethanol to Ethylene. *Microporous Mesoporous Mater.* **2008**, *116* (1), 210–215. https://doi.org/10.1016/j.micromeso.2008.04.004.
(82) Phung, T. K.; Lagazzo, A.; Rivero Crespo, M. Á.; Sánchez Escribano, V.; Busca, G. A Study of Commercial Transition Aluminas and of Their Catalytic Activity in the Dehydration of Ethanol. *J. Catal.* **2014**, *311*, 102–113. https://doi.org/10.1016/j.jcat.2013.11.010.
(83) Kwak, J. H.; Mei, D.; Peden, C. H. F.; Rousseau, R.; Szanyi, J. (100) Facets of γ-Al2O3: The Active Surfaces for Alcohol Dehydration Reactions. *Catal. Lett.* **2011**, *141* (5), 649–655. https://doi.org/10.1007/s10562-010-0496-8.
(84) Styskalik, A.; Kordoghli, I.; Poleunis, C.; Delcorte, A.; Dochain, D. D.; Moravec, Z.; Vida, J.; Homola, T.; Aprile, C.; Fusaro, L.; Devred, F.; Debecker, D. P. Non-Hydrolytic Sol–Gel Route to a Family of Hybrid Mesoporous Aluminosilicate Ethanol Dehydration Catalysts. *J. Mater. Sci.* **2021**, *56* (25), 14001–14018. https://doi.org/10.1007/s10853-021-06166-9.
(85) Marquez, A. G.; Horcajada, P.; Grosso, D.; Ferey, G.; Serre, C.; Sanchez, C.; Boissiere, C. Green Scalable Aerosol Synthesis of Porous Metal–Organic Frameworks. *Chem. Commun.* **2013**, *49* (37), 3848–3850. https://doi.org/10.1039/C3CC39191D.

Supporting Information

# Coupling of Solvent-free synthesis and reactive extrusion of alumina: an ecologically efficient integration for heterogeneous catalysts synthesis

*AUTHOR NAMES*

*Pierre-Igor Dassie [‡1], Ryma Haddad [‡1], Maud Lenez[1], Alexandra Chaumonnot[2], Malika Boualleg[2], Patrick Legriel[1], Ales Styskalik[4], Bernard Haye[1], Mohamed Selmann[3], Damien P. Debecker[4], Clement Sanchez[1], Corinne Chaneac[1] and Cedric Boissiere[1]*.*

AUTHOR ADDRESS

1. Laboratoire de Chimie de la Matière Condensée de Paris (LCMCP), Collège de France Sorbonne Université, CNRS, 4 Place Jussieu, 75252 Paris, France.
2. IFP Energies Nouvelles (IFPEN), BP 3, F-69360 Solaize, France.
3. Fédération de Chimie et Matériaux de Paris-Centre (FCMat) Sorbonne Université, Paris France.
4. Institute of Condensed Matter and Nanosciences (IMCN), Université catholique de Louvain (UCLouvain), Place Louis Pasteur, 1, 1348 Louvain-La-Neuve, Belgium).

**Scamex's Twin Screws Micro-Extruder (TSME)**

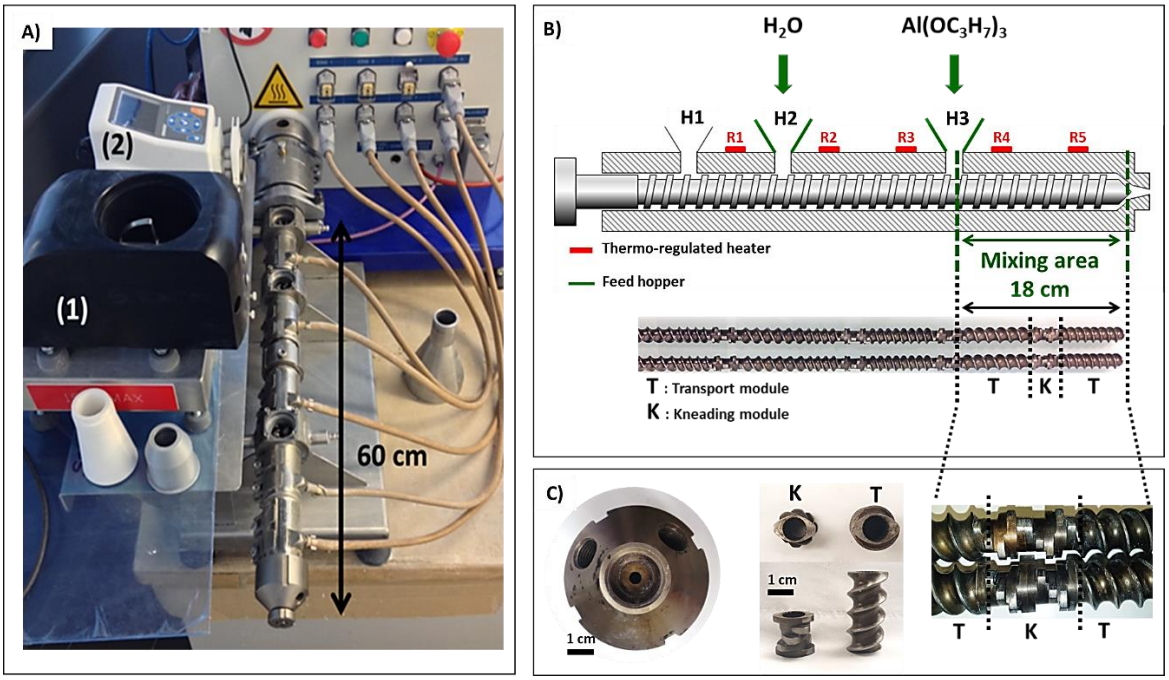


*SI. 1.* ***A) TSME picture with the doser (1) and the peristaltic pump (2); B) scheme of the experimental set up associated with the picture of screws design; C) Zoom into the extruder head with 0.5 cm orifice size, in the left, and zoom into screw profil: kneading module 1.8 X 1.8 cm and the transport module 1.8 x 3.5 cm.***

**Aluminium isopropoxide XRD diffractogram**

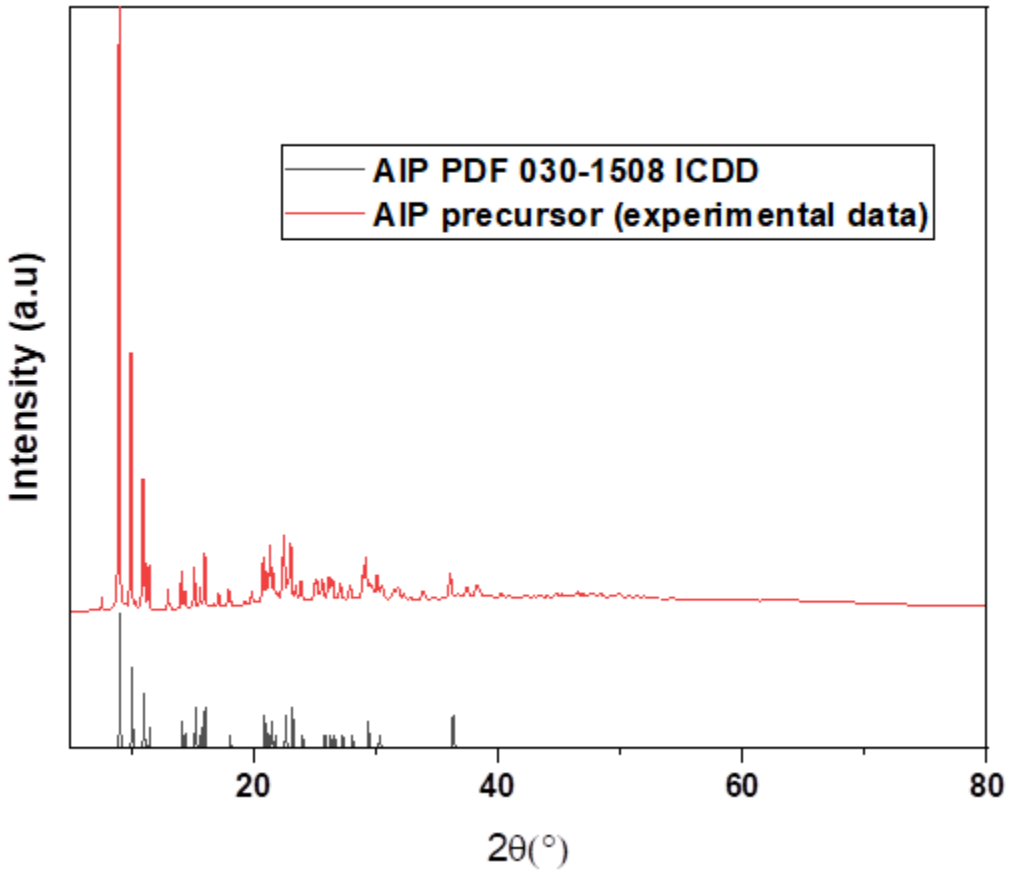


**SI. 2.** XRD pattern of AIP precursor.

**Microtome TEM picture**

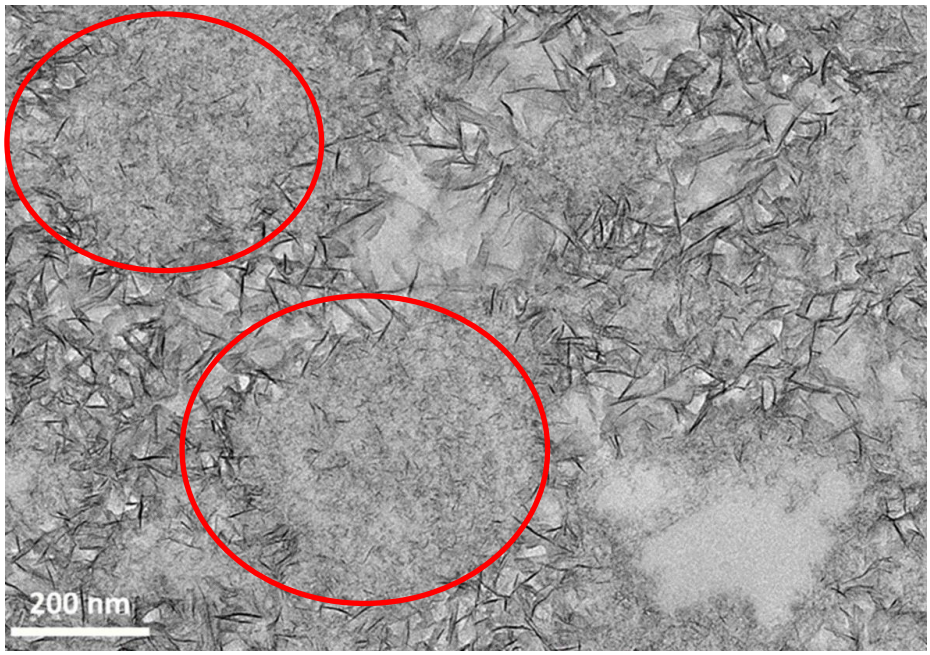


*SI. 3.* ***Microtome TEM picture of RE_AIP_8_ D sample, presence of some heterogeneous domains of small platelets.***

**Nitrogen physisorption isotherms of the extrudates**

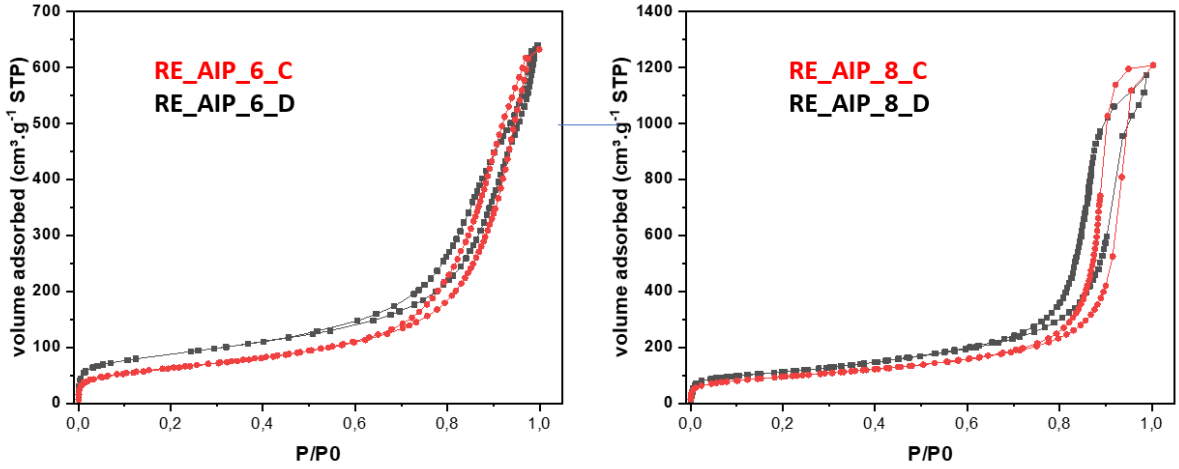


*SI. 4.* ***Nitrogen adsorption-desorption isotherms, recorded at 77 K, for samples with hydrolysis rate h= and h=8. The dried extrudates are represented in black and extrudates calcined at 540 °C are represented in red.***

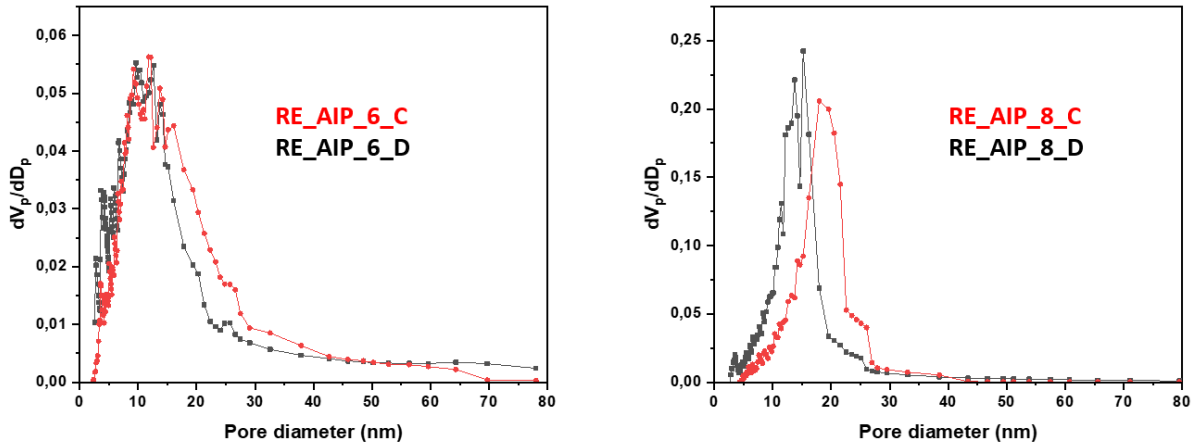


*SI. 5.* ***Pore size distribution curves for samples with hydrolysis rate h=6 and h=8. The dried extrudates are represented in black and extrudates calcined at 540 °C are represented in red.***

**Characterization of the extrudates made by the kneading extrusion pathway**

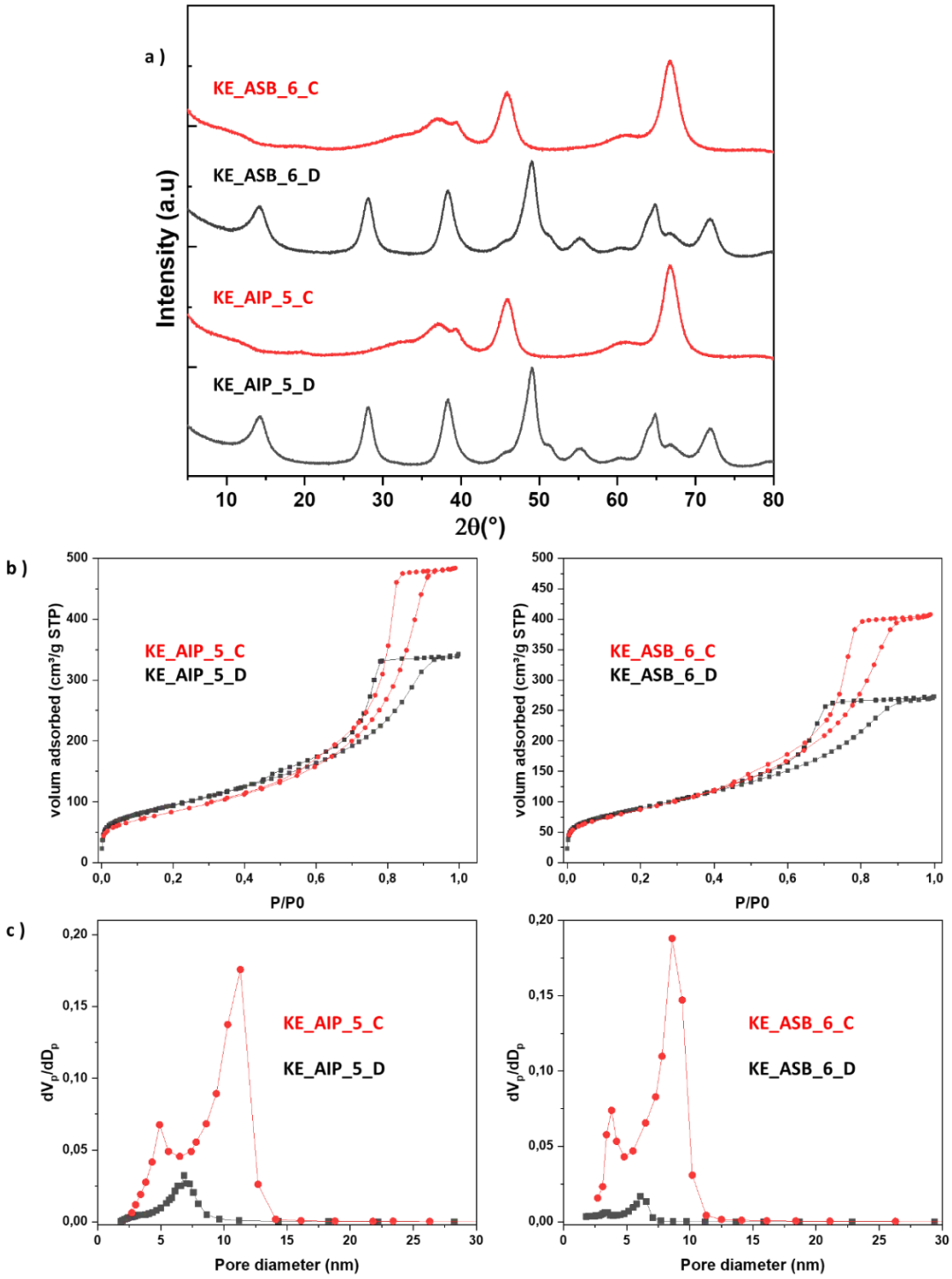


*SI. 6.* ***Characterization of the extrudates obtained in batch synthesis by sol-gel solvent-free synthesis and shaped in a second time by the usual kneading, peptisation, neutralization, followed by extrusion pathway. Analyses are performed before and after calcination. The obtained extrudates before***

***calcination are labeled with D (D stands for Dry), extrudates after calcination are labeled with C and ASB stands for Aluminum tri-Sec-Butoxide. a) XRD pattern; b) $N_2$ physisorption isotherms; c) Pore size distribution curves.***

*Catalytic stability during ethanol dehydration catalytic test*

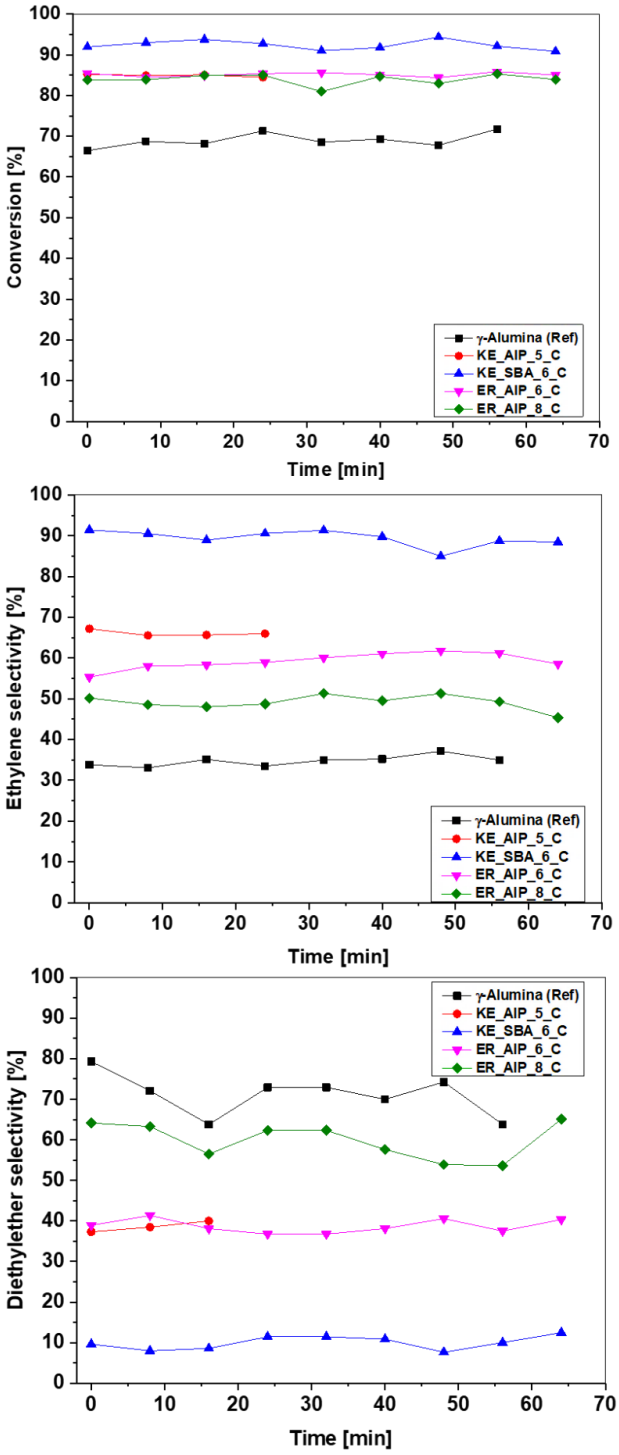


**SI. 7.** Time-on-stream evolution of ethanol conversion and Ethylene and Diethyl Ether selectivity for the tested samples at 255 °C.